



Discovery of novel inhibitors of human phosphoglycerate dehydrogenase by activity-directed combinatorial chemical synthesis strategy

Xia Zhou^{a,1}, Yuping Tan^{a,1}, Kun Gou^{a,1}, Lei Tao^a, Yuan Luo^a, Yue Zhou^a, Zeping Zuo^a, Qingxiang Sun^{a,*}, Youfu Luo^{a,*}, Yinglan Zhao^{a,b,*}

^a State Key Laboratory of Biotherapy and Cancer Center, West China Hospital, West China Medical School, Sichuan University, and Collaborative Innovation Center for Biotherapy, Chengdu 610041, China

^b West China School of Pharmacy, Sichuan University, Chengdu 610041, China

ARTICLE INFO

Keywords:

Serine synthesis
3-phosphoglycerate dehydrogenase
Inhibitor
Combinatorial chemical synthesis

ABSTRACT

Serine, the source of the one-carbon units essential for *de novo* purine and deoxythymidine synthesis plays a crucial role in the growth of cancer cells. Phosphoglycerate dehydrogenase (PHGDH) which catalyzes the first, rate-limiting step in *de novo* serine biosynthesis has become a promising target for the cancer treatment. Here we identified **H-G6** as a potential PHGDH inhibitor from the screening of an in-house small molecule library based on the enzymatic assay. We adopted activity-directed combinatorial chemical synthesis strategy to optimize this hit compound. Compound **b36** was found to be the noncompetitive and the most promising one with IC₅₀ values of $5.96 \pm 0.61 \mu\text{M}$ against PHGDH. Compound **b36** inhibited the proliferation of human breast cancer and ovarian cancer cells, reduced intracellular serine synthesis, damaged DNA synthesis, and induced cell cycle arrest. Collectively, our results suggest that **b36** is a novel PHGDH inhibitor, which could be a promising modulator to reprogram the serine synthesis pathway and might be a potential anticancer lead worth further exploration.

1. Introduction

Metabolic reprogramming is one of the most significant features in the development of cancers [1]. Cancer support growth and proliferation by altering their glucose uptake, aerobic glycolysis, and folate-dependent one-carbon units (1C) metabolism [2]. Otto Warburg pointed out that the rate of aerobic glycolysis of proliferating cancer cells was higher than that of normal cells, which mainly relied on oxidative phosphorylation of glucose-fuel mitochondria to generate energy [3]. This abnormal metabolic pattern was called “the Warburg effect,” and the elevated glucose consumption is still considered a marker of cancer cells. Serine is the predominant source of 1C carried by tetrahydrofolate, which provides methyl groups to modify lipids, nucleic acids, and proteins [4]. Serine metabolism is often dysregulated in cancer, which is essential for the occurrence and development of cancers.

Cells can obtain serine not only from exogenous sources through amino acid transporters [5] but also from a branch of glycolysis through the classical serine synthesis pathway (SSP) (Fig. 1) [6]. The cells transfer the glycolysis intermediate 3-phosphoglyceride (3-PG) into the serine synthesis pathway and eventually converts serine to glycine and generates a one-carbon unit, which enable cancer cells proliferation by supporting purine and pyrimidine biosynthesis [7]. Firstly, 3-phosphoglycerate dehydrogenase (PHGDH) catalyzes glycolytic intermediate 3-PG transformed into 3-phosphohydroxy pyruvate (3-PPyr), with nicotinamide adenine dinucleotide (NAD⁺) as a cofactor. Subsequently, 3-PPyr is converted to 3-phosphoserine (3-Pser) and alpha-ketoglutarate (αKG) by phosphoserine aminotransferase (PSAT) with glutamate as the nitrogen donor, and then to serine by the action of phosphoserine phosphatase (PSPH). Finally, serine hydroxymethyltransferase (SHMT) catalyzes serine and tetrahydrofolate (THF) into glycine and 5,10-methylene-THF.

Abbreviations: SSP, serine synthesis pathway; 1C, one-carbon units; 3-PG, 3-phosphoglyceride; PHGDH, 3-phosphoglycerate dehydrogenase; 3-PPyr, 3-phosphohydroxy pyruvate; NAD⁺, nicotinamide adenine dinucleotide; αKG , alpha-ketoglutarate; PSAT, phosphoserine aminotransferase; SHMT, serine hydroxymethyltransferase; THF, tetrahydrofolate; D-2-HG, D-2-Hydroxyglutarate; ADS, activity-directed synthesis.

* Corresponding authors at: State Key Laboratory of Biotherapy and Cancer Center, West China Hospital, West China Medical School, Sichuan University, and Collaborative Innovation Center for Biotherapy, Chengdu 610041, China (Y. Zhao).

E-mail addresses: sunqingxiang@hotmail.com (Q. Sun), luo_youfu@scu.edu.cn (Y. Luo), zhaoyinglan@scu.edu.cn (Y. Zhao).

¹ These authors made equal contribution to this work.

<https://doi.org/10.1016/j.bioorg.2021.105159>

Received 5 April 2021; Received in revised form 4 July 2021; Accepted 6 July 2021

Available online 8 July 2021

0045-2068/© 2021 Published by Elsevier Inc.

PHGDH is the first and only rate-limiting enzyme in the SSP, which is considered one of the ways for cancer cells proliferation and stress resistance [8]. Focal amplifications of the gene encoding PHGDH have been identified, and the mRNA and protein levels of PHGDH were significantly increased, particularly in breast cancers and melanomas [9–11]. Notably, PHGDH overexpressed in 40% of melanoma and 70% of estrogen receptor-negative and triple-negative breast cancer [12]. In breast cancer, melanoma, glioma, colon cancer, cervical cancer, pancreatic cancer, non-small cell lung cancer (NSCLCs), and ovarian cancer, the amplification and overexpression of PHGDH were associated with poor prognosis and short overall survival rate [13–17]. In most cases, increased PHGDH levels promote cancer cell proliferation, which is inhibited when PHGDH is knocked out or mutated at specific sites. PHGDH has been further demonstrated to use α -ketoglutarate as a substrate to produce cancer metabolite D-2-Hydroxyglutarate (D-2-HG), which is essential for the proliferation, invasion, and tumorigenicity of cancer cells [18]. Together these findings suggest that PHGDH is an attractive antitumor target, and the development of PHGDH inhibitors will open a new way for cancer treatment.

In recent years, several compounds have been reported to inhibit PHGDH, which can be divided into two categories (Fig. 2). The first category is allosteric inhibitors, such as CBR-5884 (1) [19], NCT-503 (2) [20], α -ketothioamide derivatives (3) [21], and PKUMDL-WQ-2201 (4) [22], which display micromolar potency and do not depend on the level of intracellular cofactors. The second category is orthosteric inhibitors, all of which are indole derivatives. Astra Zeneca discovered a series of indole-2-carboxamide compounds (1) that binds the NAD^+ pocket of PHGDH and inhibit its activity with low nanomolar affinities [23]. Due to structural similarity, compound (6) of RAZE is likely to share the same binding mode as compound (1) [24]. Boehringer Ingelheim [25] discovered another indoleamine compound, BI-4916 (8), a prodrug of the cofactor nicotinamide adenine dinucleotide (NADH/NAD^+)-competitive PHGDH inhibitor BI-4924 (7), which combines with NAD^+ competitive pocket and inhibits PHGDH activity at nanomolar concentration. Nevertheless, the chemical structure types of PHGDH inhibitors are quite limited, and most of them have moderate cell activity. There is a pressing need to develop inhibitors with new scaffold structure and antitumor activity.

The traditional modification iteration of the hit compound (s)

includes design, synthesis, separation, purification, and biological evaluation, which is time-consuming, uneconomical, and less environmentally friendly [26]. Although it is still widely used drug candidates' discovery, these shortcomings limit its use on a broader scale. The emergence of activity-directed synthesis (ADS), a novel discovery approach in which bioactive molecules and related synthesis appear simultaneously, has expanded the diversity of small molecule screening collections [27]. The integration of synthesis and assay significantly reduce material requirements and achieve rapid analysis. Combinatorial chemistry strategy can combine different building blocks with a one-pot reaction to obtain structurally diverse libraries of compounds [28]. Herein we report an activity-directed combinatorial chemical synthesis strategy to obtain novel PHGDH inhibitors as promising anticancer drug candidates.

2. Results and discussion

2.1. Identification of H-G6 as a PHGDH inhibitor.

To identify small molecules inhibiting human PHGDH, we screened an in-house library of 2680 compounds by using an *in vitro* enzymatic activity assay (Fig. 3A). Initially, compounds were tested at a single concentration of 5 μM to inhibit PHGDH, and we selected 70 compounds with an inhibition ratio of over 80% for diaphorase counter-screening analysis to exclude false-positive results. 48 compounds were obtained and we verified compounds' activity and got the hit compound H-G6 which exhibited a significant inhibition against PHGDH activity with the inhibition ratio >50% at 1 μM , and IC_{50} value of $4.57 \pm 0.29 \mu\text{M}$.

2.2. Optimization of hit compound H-G6 through the activity-directed combinatorial chemical synthesis strategy

To prepare a series of H-G6 analogs rapidly and economically, we used the activity-directed combinatorial chemical synthesis strategy to advance structure optimization (Fig. 4A). We selected 10 types I substituent building blocks and 10 types II internal substituent building blocks for the micro-one-pot aldol condensation experiment (Fig. 4C) by purchasing or synthesizing (The chemical synthesis method of the intermediates is shown in Scheme 1). All reactions were carried out in PCR

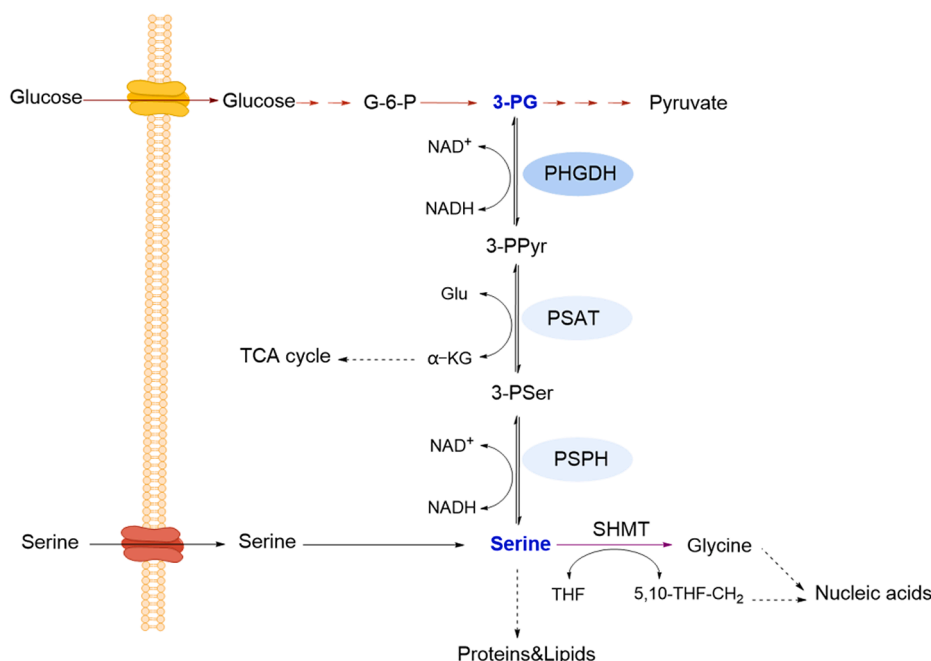


Fig. 1. The serine synthesis pathway and downstream anabolic reactions of serine.

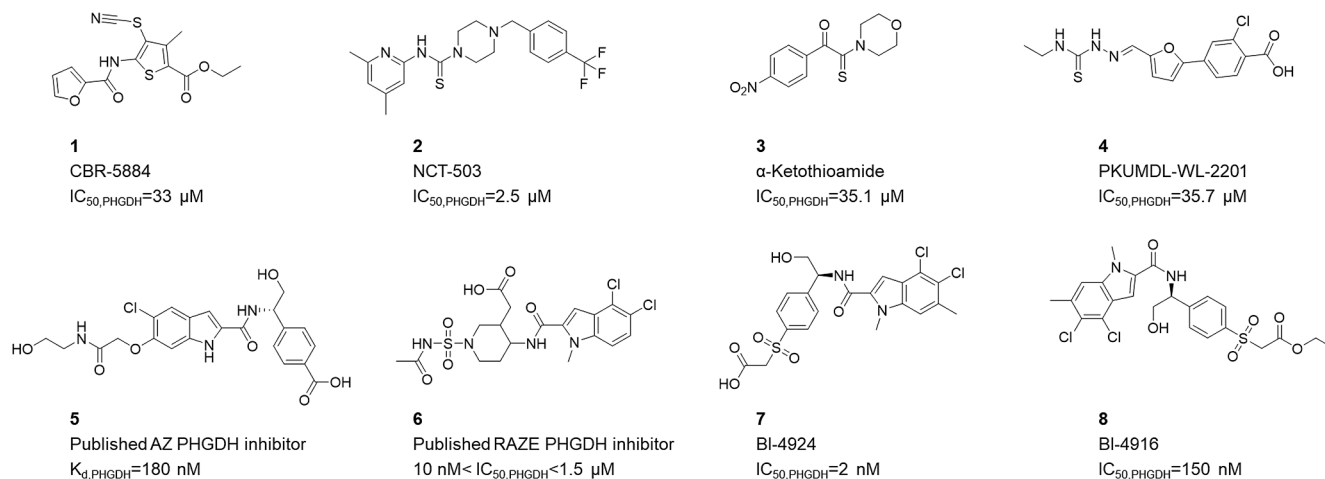
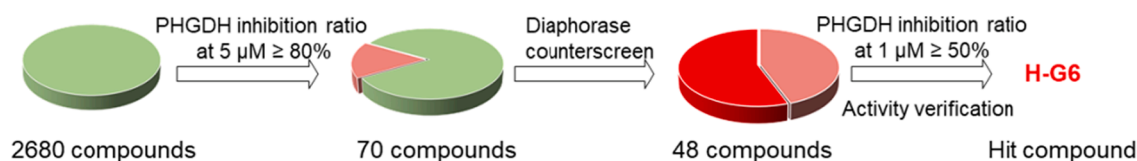
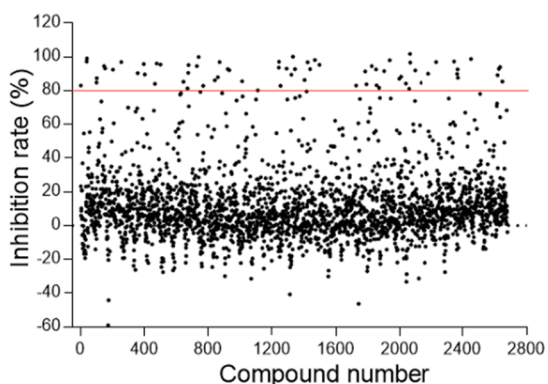


Fig. 2. The chemical structures of reported PHGDH inhibitors.

A



B



C

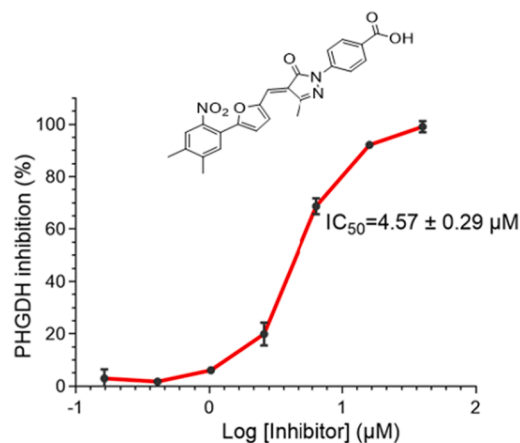


Fig. 3. Identification of a novel PHGDH inhibitor H-G6 from the chemical library screen. (A) The workflow for the identification of novel PHGDH inhibitors in an in-house library. (B) A random screen of 2680 compounds identified compounds with the inhibition ratio $>80\%$ at $5 \mu M$. (C) Chemical structure and enzymatic inhibition curve of the hit compound H-G6.

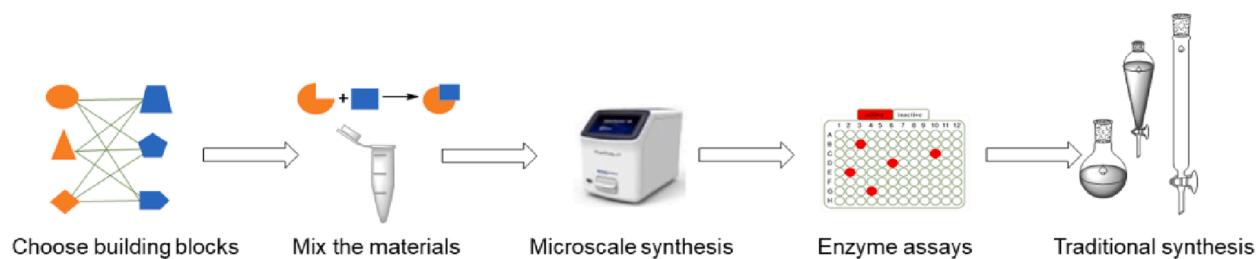
tubes at $50 \mu L$ scale and heated by qPCR instrument. Eventually, 480 (8×60) crude products were obtained by micro-one-pot synthesis, and the PHGDH enzymatic activity at a single-point concentration of $5 \mu M$ was determined. The building block had no inhibitory effect on PHGDH at this concentration. Finally, we inferred the preliminary structure – activity relationship (SAR) from 480 crude products obtained from the microscale combination screening. The compounds with *para*-substituted benzene ring in moiety I exhibited better inhibitory activity, and $-COOCH_3 > \text{halogens} > \text{no substitutions} > -COOH$. Compounds

with *meta* or *para* electron-donating groups and hydrophobic groups at moiety II exhibited strong inhibition potency.

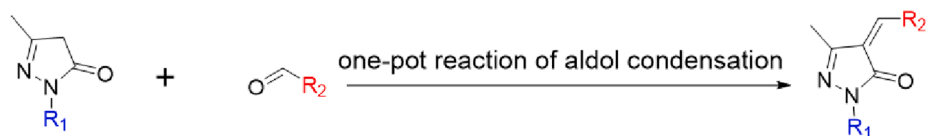
2.3. Biological activity assay of the optimized compounds

The products with high PHGDH inhibitory activity were screened from 480 one-pot reactions for routine synthesis, structure confirmation, and activity determination. Firstly, we repeated the micro-synthesis by the traditional method and then separated and purified the reaction

A



B



C

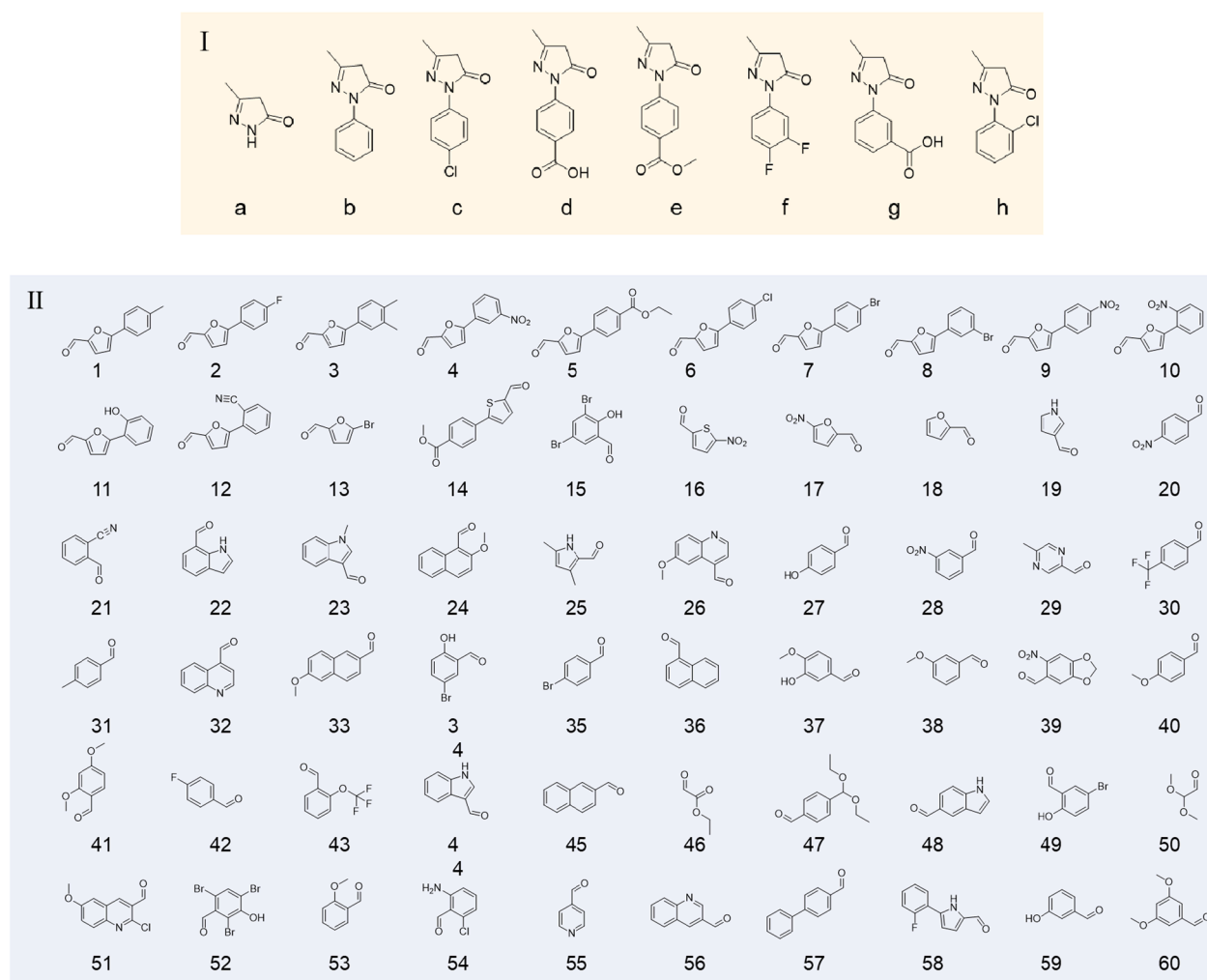
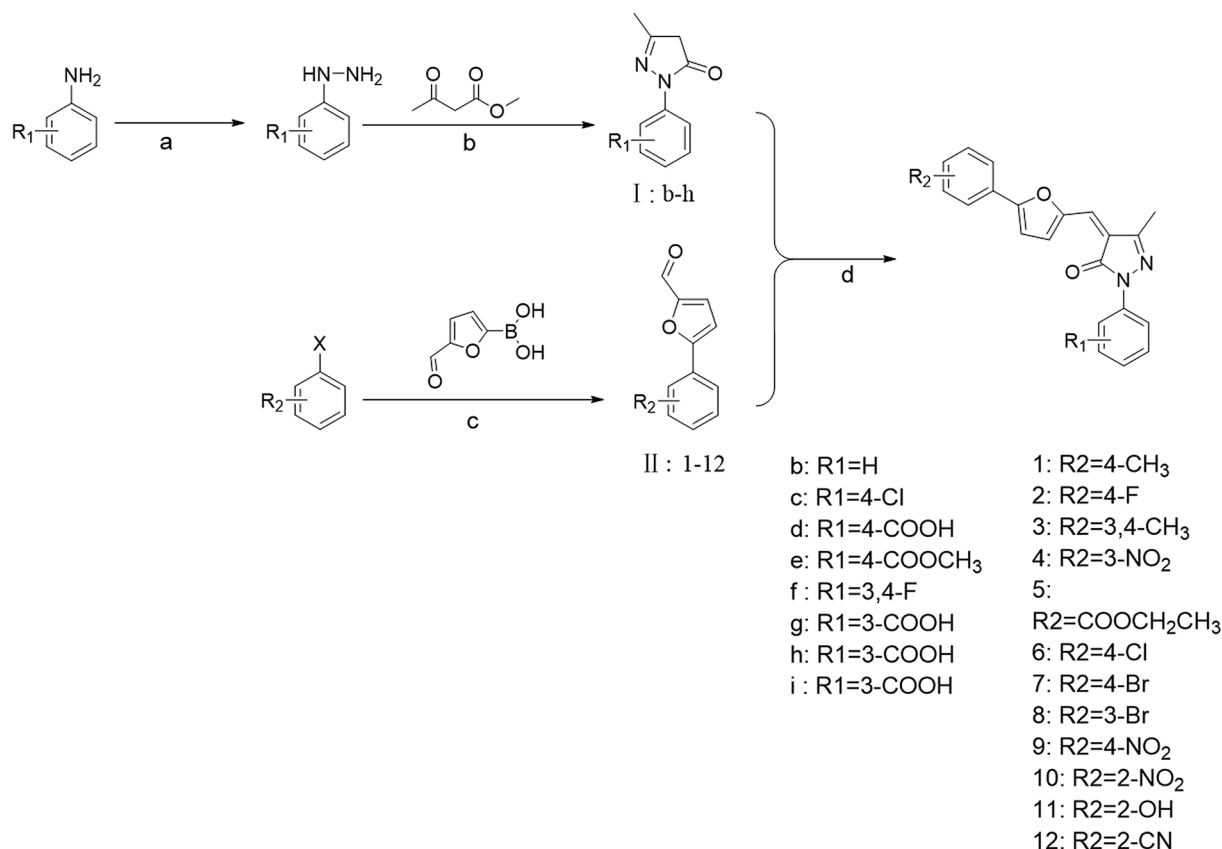


Fig. 4. Structural optimization of H-G6 through the activity-directed combinatorial chemical synthesis strategy. (A) The workflow for structural optimization by combinatorial chemical synthesis. (B, C) Micro-one-pot aldol condensation and building blocks for moieties I and II for the combinatorial chemical.



Scheme 1. Synthetic route for building blocks. Reagents and conditions: (a) NaNO₂, HCl, SnCl₂ · HCl, -10 °C; (b) CH₃CO₂H, 100 °C, overnight; (c) (pph)₃pdCl₂, CH₃COOK, dioxane : H₂O = 3 : 1, N₂, 90 °C, overnight; (d) DMSO (micro-one-pot synthesis) or EtOH (traditional synthesis), CH₃CO₂H, 55 °C, 3 h.

liquid to obtain two main products. One is the aldol reaction adduct; other is the bis-pyrazolone derivative (Scheme 2). As we used activity-directed synthesis, the reaction products may be PHGDH inhibitors. The enzymatic activity assay revealed that all these compounds displayed potent inhibitory activity against PHGDH. The enzymatic inhibitory activities of monomer adducts and their corresponding bis-pyrazolone derivatives were in the same order of magnitude. In order to exclude non-specific binding, we selected compounds **H-G6**, **b36**, and **bis-b36** for false positive and non-specific binding exclusion experiments, because they have three representative structures. The result showed that all the compounds did not inhibit the activity of diaphorase, and the addition of Triton X-100 did not weaken the inhibition activity of the compounds against PHGDH (Figure S1), confirming that these compounds are inhibitors of PHGDH. However, bis-pyrazolone derivatives had higher molecular weight, lower ligand efficiency and poor water solubility. Since all of the optimized compounds exhibited considerable PHGDH inhibition activity in extracellular enzyme assay, we evaluated their antiproliferative activity against a panel of human cancer cell lines including human breast cancer cells MDA-MB-468 and Hs578T, and human ovarian cancer cells A2780 and SKOV3 after 96 h treatment. The results showed that compounds **H-G6**, **b16**, **b36**, and **bis-b36** displayed dominant antiproliferative activity at 20 μM against cancer cells (Table 1).

2.4. Cell proliferation inhibitory assay of compounds

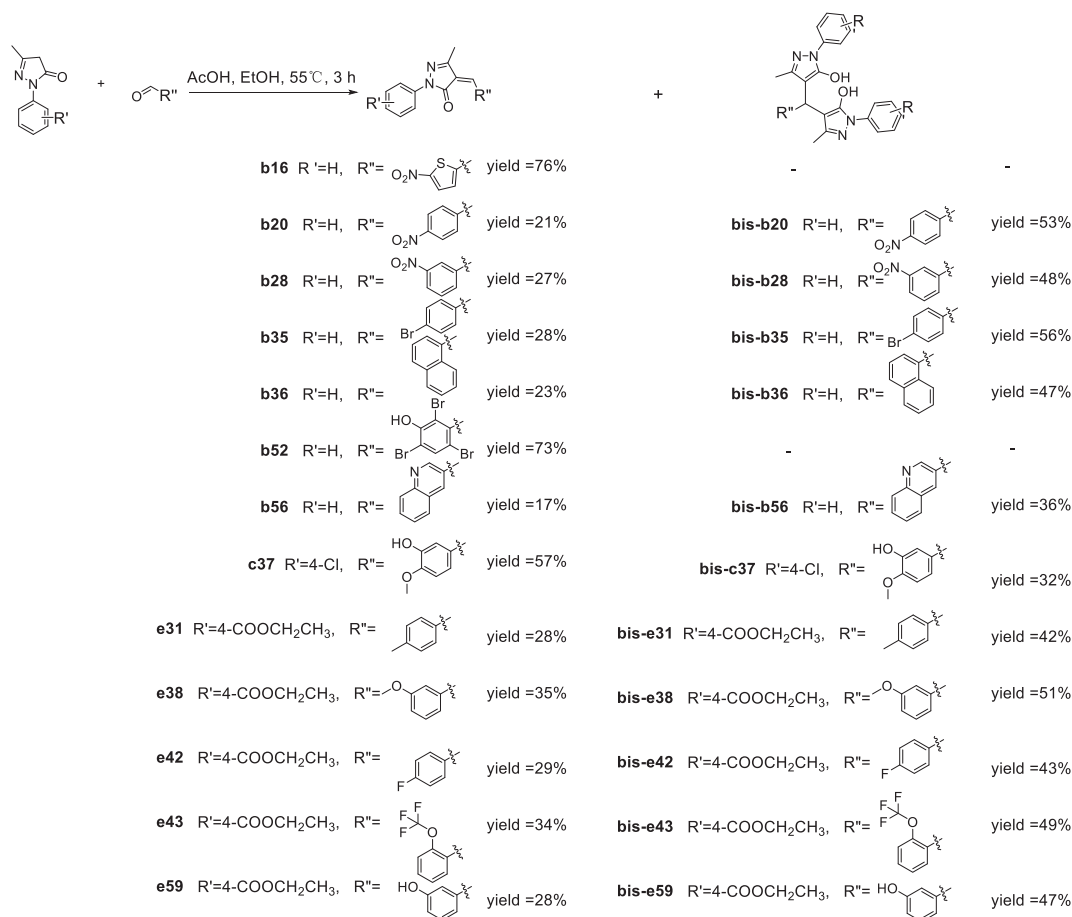
As compounds **H-G6**, **b16**, **b36**, and **bis-b36** displayed dominant antiproliferative activity at 20 μM against cancer cells, we further investigated their antiproliferative activities in various concentrations after 96 h exposure using the MTT assay. The results showed that they inhibited the breast cancer cells proliferation with IC₅₀ value of 12.97–33 μM. Notably, compounds exhibited stronger inhibition against

ovarian cells (A2780 and SKOV3) with IC₅₀ value of 2.69–18.76 μM than that of breast cancer cells, suggesting the possible important role of PHGDH in the pathogenesis of ovarian cancer (Table 2). The difference sensitive of cancer cells to compounds may be the difference of gene expression in cancer cells. Thus, the mechanism by which ovarian cancer cells sensitive to PHGDH inhibitor is worthy further study. In addition, we measured the toxicity of these compounds on normal cells and the results showed that high concentration (40 μM) of compounds **b36**, **bis-b36** and **H-G6** didn't significantly inhibit the proliferation of MCF-10A, suggesting that these compounds are nontoxic to normal cell and specifically inhibit the cancer cells proliferation. In summary, these compounds are more selective for tumor cells than normal cells.

Absorption, distribution, metabolism, elimination, and toxicity (ADMET) are very important in current drug discovery and development. In silico assessment of ADMET predictions of these active compounds were carried out using Qikprop (Schrodinger Small-Molecule Drug Discovery Suite) (Table S1). Compound **b36** exhibited more "drug-like" e⁺ properties and was selected for further study.

2.5. Formate supplementation rescue experiment

Formic acid (FA) is a crucial one-carbon metabolite of serine, which generates 10-formyl tetrahydrofuran in cells and participates in the synthesis of purine nucleotides [29]. As the inhibition of PHGDH activity reduced the serine and pyrimidine nucleotide synthesis vital for cancer cell proliferation, supplementation of exogenous FA in cancer cells could rescue the proliferation inhibitory effects of PHGDH inhibitors. MDA-MB-468 cells were treated with compound **b36** with or without formate supplementation, the result indicated that the addition of 1 mM formate recovered the proliferation inhibition of MDA-MB-468 induced by **b36**, especially 5 days after **b36** treatment (Fig. 5).



Scheme 2. Traditional methods synthesized the optimized compounds.

2.6. Cell metabolism studies

As **b36** inhibited PHGDH activity, we then determined whether **b36** inhibited *de novo* biosynthesis of serine synthesis in cancer cells. The level of serine and its downstream glycine in MDA-MB-468 cells after **b36** treatment was determined by using a targeted reversed-phase gradient UPLC-MS/MS assay method for quantitative/monitoring of intracellular amino acids established by the precolumn derivation of 6-aminoquinolyl-*N*-hydroxysuccinimidyl carbamate (AccQTag Ultra) [30]. The results showed that **b36** significantly decreased the serine and glycine level in a concentration-dependent manner, suggesting that PHGDH inhibition by **b36** inhibited the *de novo* synthesis of serine (Fig. 6).

2.7. DNA damage studies

Inhibition of serine synthesis reduces the synthesis of purine nucleotides, which are the main components of DNA. The DNA synthesis ability of MDA-MB-468 cells treated with **b36** was determined by 5-Ethynyl-20-deoxyuridine (EdU) incorporation. EdU is a thymidine nucleoside analog that can replace thymidine in cell proliferation. Based on the specific reaction of EdU with fluorescent dyes and azido biotin, the synthesis of DNA in cells is detected, which reflect the inhibition of cell proliferation [31]. The results showed that **b36** significantly inhibited the production of intracellular DNA in MDA-MB-468 cell in a concentration-dependent manner, suggesting DNA synthesis was damaged (Fig. 7). For example, 20 μ M of **b36** treatment resulted in 70% inhibition of DNA production, which is consistent with the PHGDH inhibition effect of **b36**.

We have confirmed that compound **b36** can inhibit DNA synthesis,

because serine synthesis and metabolism can provide a carbon unit for the synthesis of purine and pyrimidine. It has been reported that siPHGDH can increase the accumulation of the DNA damage marker histone H2AX on Ser139 (generally referred to as γ H2AX) [32]. We hypothesize that the same effect can be achieved by inhibiting PHGDH with our compounds. Western blot experiment showed that **b36** markedly increased the level of γ H2AX in MDA-MB-468 cells in a dose-dependent manner (Fig. 8A). We then found that the accumulation of γ H2AX foci was also significantly increased in MDA-MB-468 cells after **b36** treatment (Fig. 8B and 8C). These data indicated that the inhibition of PHGDH in tumor cells accumulate DNA strand breaks.

2.8. Cell cycle arrest analysis

A series of biological processes such as cell proliferation, growth, and differentiation are regulated by the cell cycle [33]. As the inhibition of PHGDH activity suppressed the formation of purine nucleotides required for DNA synthesis, we speculated that **b36** treatment may result in cell cycle arrest. Thus, we investigated the effect of **b36** on the cell cycle of MDA-MB-468 by flow cytometry. The results showed that **b36** at 40 μ M induced cell cycle arrest of the MDA-MB-468 cell at S-phase, which is consistent with DNA synthesis inhibition (Fig. 9).

2.9. Analysis of compounds inhibition modality

We sought to deeply characterize the mechanism by which compounds inhibit PHGDH, and look for the pockets where they bind to the enzyme. We selected compounds **H-G6**, **b36**, and **bis-b36** to perform an enzyme kinetics study to explore the mode of inhibition, because they have three representative structures [33]. Competition studies showed

Table 1

The PHGDH inhibitory activity and preliminary cancer cell proliferation inhibitory activity of the active compounds.

Compound	Inhibitory activity (IC ₅₀ , μM) ^a	Antiproliferative activity (Inhibition rate at 20 μM) ^b			
		PHGDH	MDA-MB-468	Hs578T	A2780
H-G6	4.57 ± 0.29	88%	50%	10%	- ^c
b16	6.39 ± 0.04	97%	12%	94%	80%
b20	4.69 ± 0.12	40%	6%	68%	31%
bis-b20	3.41 ± 0.18	11%	10%	-	6%
b28	5.38 ± 0.51	39%	13%	3%	3%
bis-b28	3.24 ± 0.05	29%	9%	4%	8%
b35	10.01 ± 0.34	20%	5%	9%	5%
bis-b35	4.36 ± 0.34	5%	-	4%	2%
b36	5.96 ± 0.61	49%	75%	89%	74%
bis-b36	7.04 ± 0.45	68%	85%	66%	29%
b52	4.52 ± 0.53	-	-	-	2%
b56	5.95 ± 0.56	19%	9%	5%	7%
bis-b56	3.12 ± 0.30	9%	6%	-	5%
c37	13.29 ± 1.99	26%	9%	-	-
bis-c37	8.9 ± 0.17	19%	-	-	-
e31	20.09 ± 1.10	-	4%	-	-
bis-e31	12.84 ± 2.21	5%	-	8%	17%
e38	6.27 ± 0.34	38%	30%	11%	12%
bis-e38	4.58 ± 0.17	16%	2%	-	5%
e42	4.58 ± 0.35	15%	29%	-	-
bis-e42	4.77 ± 0.04	7%	-	-	-
e43	9.33 ± 0.37	13%	-	13%	29%
bis-e43	6.12 ± 1.01	21%	9%	-	28%
e59	3.95 ± 0.29	-	12%	-	0%
bis-e59	4.79 ± 0.71	-	-	1%	3%

^a Each compound was tested in triplicate; the data are presented as the mean ± SD.

^b Cell proliferation inhibition at a single concentration.

^c Compounds had no proliferation inhibition.

Table 2

IC₅₀^a value (μM) of compounds against cancer and normal cell lines.

Compound	MDA-MB-468	Hs578T	A2780	SKOV3	MCF-10A
H-G6	27.24 ± 0.84	33.55 ± 2.93	2.69 ± 3.22	4.14 ± 3.92	>40.00
	12.97 ± 1.37	> 40.00	5.60 ± 0.28	6.38 ± 0.90	38.95 ± 0.91
b36	31.13 ± 0.53	24.00 ± 0.39	8.99 ± 0.19	18.76 ± 5.10	>40.00
	31.59 ± 0.45	22.42 ± 0.58	9.9 ± 2.01	8.462 ± 3.32	>40.00

^a Each compound was tested in triplicate; the data are presented as the mean ± SD.

that all the compounds inhibited PHGDH in a non-competitive mode with respect to both 3-PG and NAD⁺, as evidenced by dose-dependent decrease in V_{max} and little effects on K_m for the substrate 3-PG and the cofactor NAD (Fig. 10), suggesting that compounds might be binding to an allosteric pocket.

3. Conclusion

In summary, we identified a potential PHGDH inhibitor H-G6 from the screening of an in-house small molecule library by *in vitro* enzymatic activity assay. To avoid the disadvantages of traditional synthesis, which is time-consuming and costly, we used the activity-directed combinatorial chemical synthesis strategy to optimize the lead compound. We designed and synthesized a series of pyrazolone derivatives as novel PHGDH inhibitors with IC₅₀ values ranging from 3.12 to 20.09 μM. Compound b36 showed potent activities with the IC₅₀ value of 5.96 ± 0.61 μM and exhibited significant antiproliferative activities against

MDA-MB-468, Hs578T, A2780, and SKOV3 cell lines, but not normal cells (MCF-10A). Mechanistically, compound b36 is an allosteric inhibitor of PHGDH, reduces intracellular serine synthesis, blocks DNA replication, leads to S phase arrest, activates DNA damage accumulation, and finally causes cell death. Collectively, our data demonstrated that b36 is a promising PHGDH inhibitor and might provide a rationale for the development of PHGDH inhibitors for cancer therapy.

4. Experimental section

4.1. General procedures

All reagents and solvents were purchased from commercial sources and were used without further purification. All the chemical reactions were monitored by thin-layer chromatography (TLC) on precoated silica gel 60 F254 plates (0.25 mm, Qingdao Haiyang Inc.), and components were visualized by ultraviolet light (254 nm). All the NMR spectra were recorded on Bruker Avance (Varian Unity Inova) spectrometer in CDCl₃ or DMSO-d₆ with TMS as internal standard. ¹H NMR and ¹³C NMR spectra were recorded respectively at 400 MHz and 100 MHz, analyzed by MestReNova Software. Coupling constants were reported as Hz with multiplicity denoted as s (singlet), d (doublet), t (triplet), q (quartet), m (multiplet), and br (broad). High-resolution mass spectrometry (HRMS) was acquired on a Waters Q-TOF Premier mass spectrometer.

4.2. Compound library

The in-house small molecular library used for the screening assay consists of 2636 commercially available pure compounds with structural diversity (Source: MedChem Express). They are stored at concentrations of 10 mM in 100% dimethyl sulfoxide (DMSO) with the purities of > 95%. The hit H-G6 from the screening assay were purchased from a local agent, confirmed by ¹H NMR and HRMS before use.

4.3. Implementation of combinatorial chemistry one-pot reaction

All reactions were carried out in PCR tubes at 50 μL scale. The reactants were dissolved in DMSO to a final concentration of 40 mM (1.0 equiv), and 0.3 μL glacial acetic acid (2.0 equiv) was added as a catalyst. The reaction mixtures were heated in a real-time PCR detection systems (Bio-Rad, CFX96) at 55 °C for 3 h, followed by cooling to room temperature.

4.4. Chemistry

4.4.1. General procedure for the synthesis of building blocks for moieties I (I b-h)

Aniline (1.0 equiv) was dissolved in conc. HCl and cooled to -10 °C, then an aqueous sodium nitrite solution (1.5 equiv) was added and stirred cold for 40 min. The newly prepared tin dichloride (3.0 equiv) hydrochloric acid solution was added to the reaction solution slowly and stirred at -10 °C for 2–3 h [34]. At the end of the reaction, the precipitate is formed and filtered, washed with water and ethyl acetate, then dried in a vacuum, and used for the next step without further purification.

The phenylhydrazine (1.0 equiv) obtained in the previous step is dissolved in an appropriate amount of glacial acetic acid and added ethyl acetoacetate (1.5 equiv) in one portion. The mixture was stirred and heated to reflux for 12 h [34]. The solution was cooled to room temperature and a precipitate was formed, followed by washing with a small amount of organic solvent and dried in a vacuum. The residue was purified by chromatography on Si gel column with DCM-MeOH.

4.4.2. General procedure for the synthesis of building blocks for moieties II (II 5 ~ 12)

A solution of the corresponding Aryl halides (1.0 equiv) and 5-formyl-2-furanboronic acid (1.5 mmol) in 1,4-dioxane: H₂O = 3 : 1

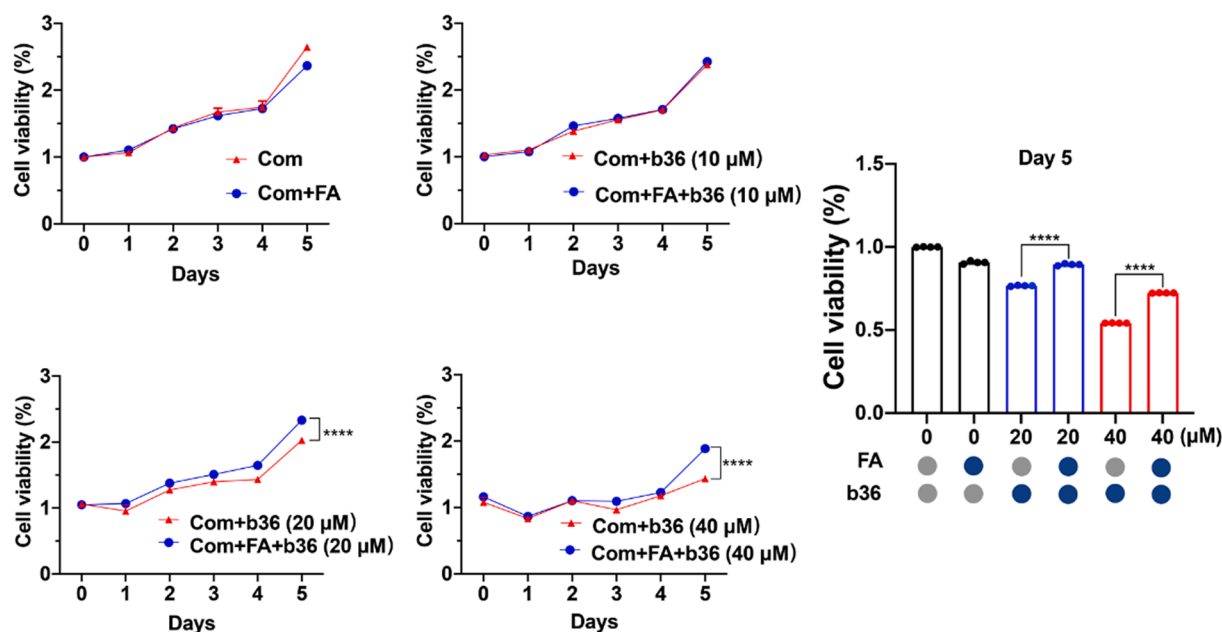


Fig. 5. Formate rescues the proliferation inhibition of MDA-MB-468 induced by b36. MDA-MB-468 cells were treated with b36 and formate (1 mM), followed by MTT assay. Statistical analysis of MDA-MB-468 cells proliferation after 5 days of treatment. The data are shown as means \pm SD. * P < 0.05; ** P < 0.01; *** P < 0.001.

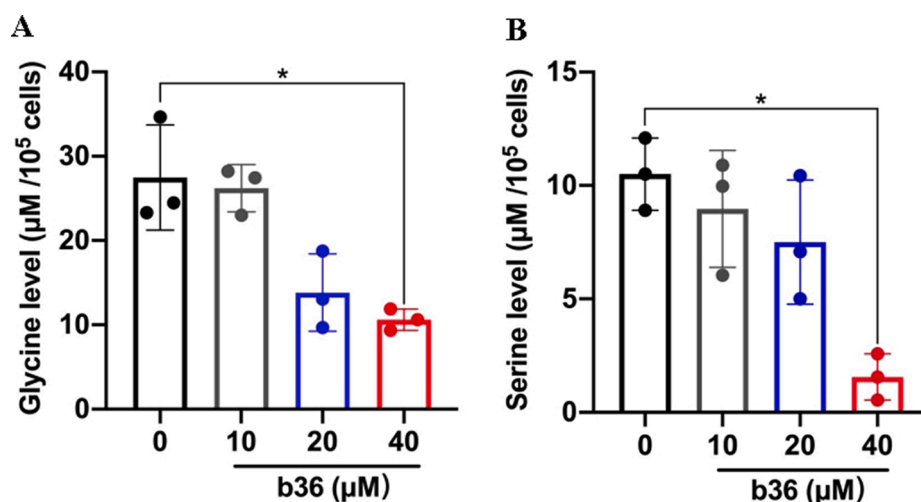


Fig. 6. Compound b36 inhibits serine synthesis in MDA-MB-468 cells. (A) The level of seine in MDA-MB-468 cells after various concentration of b36 treatment. (B) The level of glycine in MDA-MB-468 cells after various concentration of b36 treatment. * P < 0.05.

were prepared with bis (triphenylphosphine) palladium (II) chloride (0.1 equiv and potassium acetate (3.0 equiv). The mixture was stirred under nitrogen and heated to 90 °C for 12 h [34]. Then the solution was diluted with H₂O and extracted with DCM for 3 times. The combined organic phase was washed with brine and dried over anhydrous Na₂SO₄, filtered and concentrated, then purified by chromatography on Si gel column with PE-EA.

I-e was synthesized from I-d by reflux esterification in anhydrous methanol and catalytic concentrated sulfuric acid. After heating to reflux with stirring for 10 h, the reaction mixture was cooled to room temperature and concentrated under reduced pressure. Finally, the crude products were purified by chromatography on Si gel column with DCM-MeOH.

4.4.3. General procedure for the synthesis of building blocks for the optimized compounds

Building blocks for moieties I (1.0 equiv), II (1.2 equiv), and acetic

acid (2.0 equiv) in ethanol were stirred at 55 °C for 3–5 h. After cooling to room temperature, the products were precipitated, filtered, and collected, then purified by column chromatography using PE-EA or MeOH-DCM as an eluent.

4.4.4. 5-Methyl-4-((5-nitrothiophen-2-yl)methylene)-2-phenyl-2,4-dihydro-3H-pyrazol-3-one (b16)

Solid, yield 76%; ¹H NMR (400 MHz, DMSO) δ 8.26 (s, 1H), 8.24 (d, J = 4.4 Hz, 1H), 8.09 (d, J = 4.4 Hz, 1H), 7.91 (d, J = 8.0 Hz, 2H), 7.47 (t, J = 8.0 Hz, 2H), 7.24 (t, J = 7.4 Hz, 1H), 2.36 (s, 3H); ¹³C NMR (101 MHz, DMSO) δ 162.02, 156.80, 151.29, 141.02, 138.18, 137.53, 129.47, 129.34, 126.35, 125.42, 118.65, 13.22; HRMS [ESI⁺]: calcd for 313.0521, C₁₅H₁₁N₃O₃S, [M + H]⁺, found, 314.0598. Purity \geq 95.0%.

4.4.5. 5-Methyl-4-(4-nitrobenzylidene)-2-phenyl-2,4-dihydro-3H-pyrazol-3-one (b20)

Solid, yield 21%; ¹H NMR (400 MHz, DMSO) δ 8.70 (d, J = 8.0 Hz,

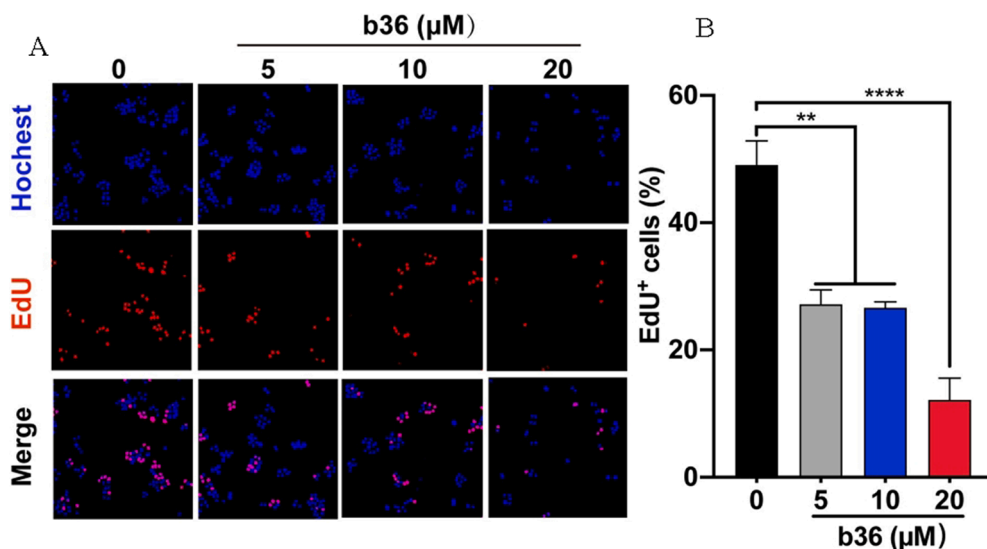


Fig. 7. Compound **b36** inhibits DNA synthesis in MDA-MB-468 cells. (A) MDA-MB-468 cells were treated with various concentrations of **b36** (5–20 μM) for 48 h and labeled by EdU (red fluorescence) and Hoechst (blue fluorescence), followed by ArrayScan VTI HCS reader detection. (B) The statistical results of DNA damage assay in MDA-MB-468 cells. The data are shown as means ± SD. ** $P < 0.01$; **** $P < 0.0001$. (For interpretation of the references to colour in this figure legend, the reader is referred to the web version of this article.)

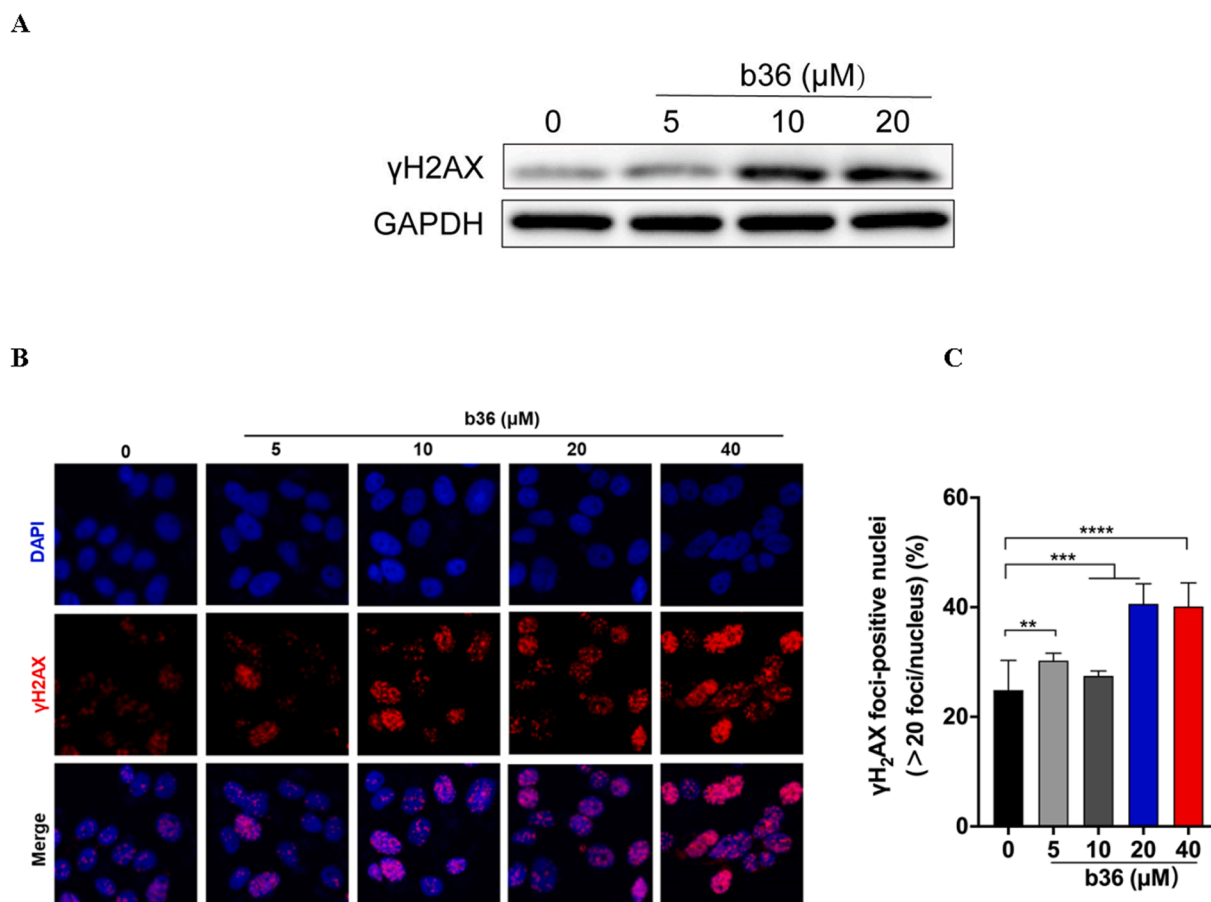


Fig. 8. Compound **b36** induces DNA damage in MDA-MB-468 cells. (A) Immunoblotting of γ H2AX after MDA-MB-468 cells were treated with compound **b36** for 48 h. GAPDH as loading control. (B, C) Representative images (B) and quantification (C) of γ -H2AX foci (red) in MDA-MB-468 cells treated with compound **b36** for 48 h. Nuclei were stained with 4,6-diamidino-2-phenylindole (DAPI, blue). The data are shown as means ± SD. *** $P < 0.001$; **** $P < 0.0001$. (For interpretation of the references to colour in this figure legend, the reader is referred to the web version of this article.)

2H), 8.37 (d, $J = 8.0$ Hz, 2H), 7.97 (s, 1H), 7.88 (d, $J = 7.5$ Hz, 2H), 7.45 (t, $J = 7.4$ Hz, 2H), 7.22 (s, 1H), 2.37 (s, 3H); ^{13}C NMR (101 MHz, DMSO) δ 161.48, 152.15, 149.37, 145.31, 138.91, 138.32, 134.56, 129.96, 129.36, 125.33, 123.84, 118.87, 13.51; HRMS [ESI +]: calcd for 307.0957 , $\text{C}_{17}\text{H}_{13}\text{N}_3\text{O}_3$, $[\text{M} + \text{H}]^+$, found, 308.1031. Purity $\geq 95.0\%$.

4.4.6. 4,4'-((4-Nitrophenyl)methylene)bis(3-methyl-1-phenyl-1H-pyrazol-5-ol) (**bis-b20**)

Solid, yield 53%; ^1H NMR (400 MHz, DMSO) δ 8.13 (d, $J = 8.8$ Hz, 2H), 7.79 (d, $J = 7.8$ Hz, 4H), 7.55 (d, $J = 8.8$ Hz, 2H), 7.38 (t, $J = 7.9$ Hz, 4H), 7.16 (t, $J = 7.4$ Hz, 2H), 4.96 (s, 1H), 2.27 (s, 6H); ^{13}C NMR

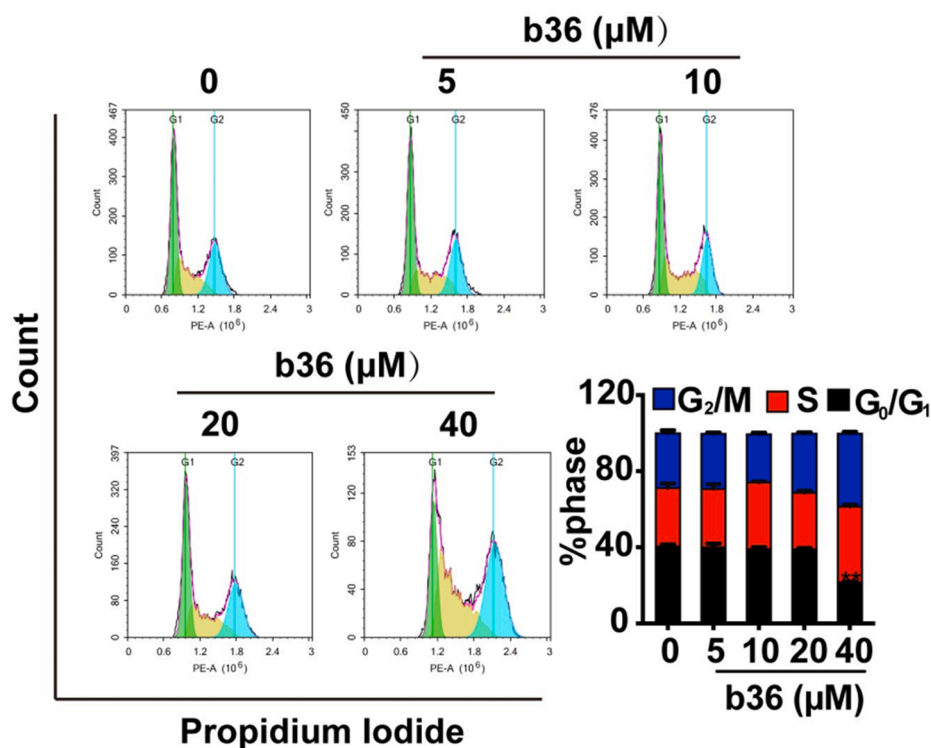


Fig. 9. Compound **b36** induces MDA-MB-468 cells arrest at S-phase. Cell cycle analysis of MDA-MB-468 cells treated with different concentrations of **b36** (5–40 μM) for 48 h. The statistical results of cell cycle assay in MDA-MB-468 cells. The data are shown as means \pm SD.

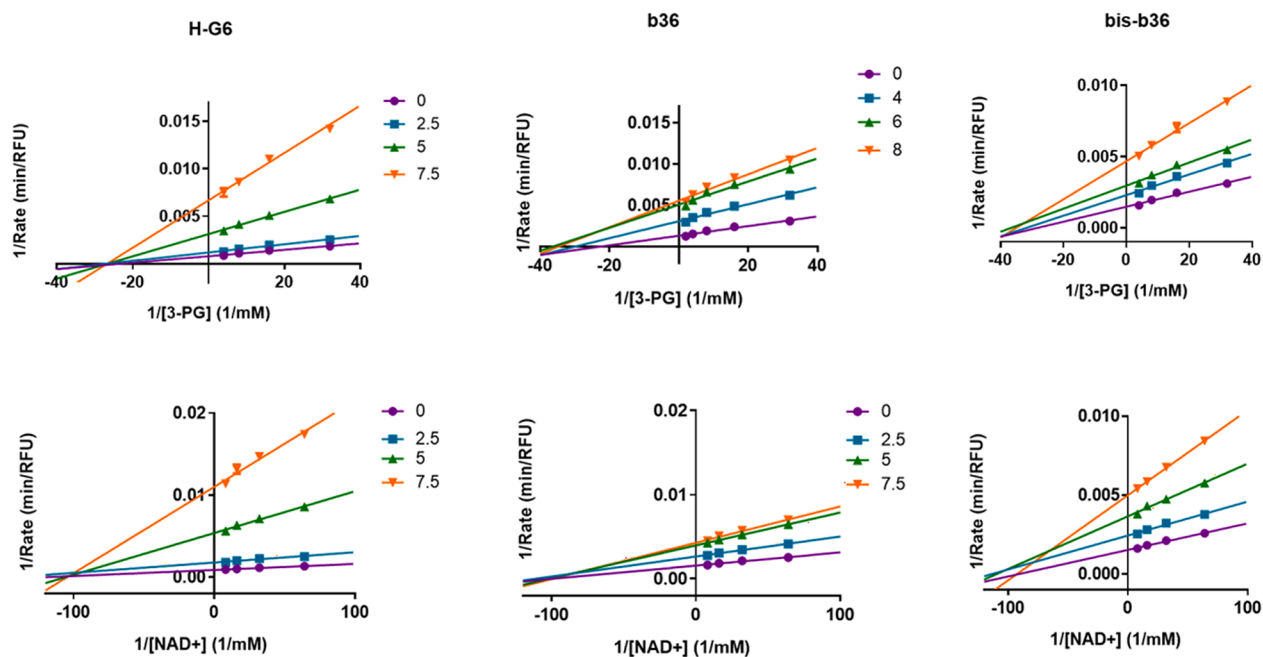


Fig. 10. Compounds exhibits non-competitive inhibition with respect to both 3-PG and NAD^+ . Data are average of three experiments and error bars represent standard deviations.

(101 MHz, DMSO) δ 157.57, 151.73, 146.61, 146.27, 138.36, 129.27, 129.06, 125.66, 123.76, 120.80, 103.80, 40.65, 40.44, 40.23, 40.02, 39.81, 39.60, 39.40, 34.03, 12.35; HRMS [ESI⁺]: calcd for 481.1750, $\text{C}_{27}\text{H}_{23}\text{N}_5\text{O}_4$, [M + H]⁺, found, 482.1825. Purity \geq 95.0%.

4.4.7. 5-Methyl-4-(3-nitrobenzylidene)-2-phenyl-2,4-dihydro-3H-pyrazol-3-one (**b28**)

Solid, yield 27%; ¹H NMR (400 MHz, DMSO) δ 9.60 (s, 1H), 8.84 (d, $J = 7.8$ Hz, 1H), 8.43 (dd, $J = 7.9, 1.8$ Hz, 1H), 8.02 (s, 1H), 7.93–7.82 (m, 3H), 7.49–7.41 (m, 2H), 7.22 (t, $J = 7.4$ Hz, 1H), 2.37 (s, 3H); ¹³C NMR (101 MHz, DMSO) δ 161.69, 152.17, 148.24, 145.80, 139.80, 138.35, 134.51, 130.56, 129.35, 129.24, 127.81, 127.28, 125.32,

118.92, 13.51; HRMS [ESI +]: calcd for 307.0957, C₁₇H₁₃N₃O₃, [M + H]⁺, found, 308.1032. Purity ≥ 95.0%.

4.4.8. 4,4'-((3-Nitrophenyl)methylene)bis(3-methyl-1-phenyl-1H-pyrazol-5-ol) (bis-b28)

Solid, yield 48%; ¹H NMR (400 MHz, DMSO) δ 8.13 (s, 1H), 8.08 (d, J = 8.1 Hz, 1H), 7.75 (d, J = 7.9 Hz, 5H), 7.60 (t, J = 7.9 Hz, 1H), 7.44 (t, J = 7.9 Hz, 4H), 7.24 (t, J = 7.4 Hz, 2H), 5.12 (s, 1H), 2.35 (s, 6H). ¹³C NMR (400 MHz, DMSO) δ 8.13 – 8.00 (m, 2H), 7.73 (t, J = 7.9 Hz, 5H), 7.60 (t, J = 7.9 Hz, 1H), 7.43 (t, J = 7.9 Hz, 4H), 7.25 (d, J = 7.4 Hz, 2H), 5.11 (s, 1H), 2.34 (s, 6H); ¹³C NMR (101 MHz, DMSO) δ 148.23, 146.70, 145.60, 138.05, 134.83, 130.10, 129.36, 125.90, 122.24, 121.56, 120.93, 104.15, 33.54, 12.24; HRMS [ESI +]: calcd for 481.1750, C₂₇H₂₃N₅O₄, [M + H]⁺, found, 482.1821. Purity ≥ 95.0%.

4.4.9. 4-(4-Bromobenzylidene)-5-methyl-2-phenyl-2,4-dihydro-3H-pyrazol-3-one (b35)

Solid, yield 28%; ¹H NMR (400 MHz, DMSO) δ 8.53 (d, J = 8.6 Hz, 2H), 7.89 (d, J = 7.7 Hz, 2H), 7.86 – 7.75 (m, 3H), 7.47 – 7.41 (m, 2H), 7.21 (t, J = 7.4 Hz, 1H), 2.35 (s, 3H); ¹³C NMR (101 MHz, DMSO) δ 161.88, 152.25, 147.26, 138.52, 135.81, 132.51, 132.23, 129.32, 127.65, 125.18, 120.57, 118.87, 13.55; HRMS [ESI⁺]: calcd for 340.0211, C₁₇H₁₃BrN₂O, [M + H]⁺, found, 341.0290. Purity ≥ 95.0%.

4.4.10. 4,4'-((4-Bromophenyl)methylene)bis(3-methyl-1-phenyl-1H-pyrazol-5-ol) (bis-b35)

Solid, yield 56%; ¹H NMR (400 MHz, DMSO) δ, 7.75 (d, J = 7.7 Hz, 4H), 7.50 – 7.34 (m, 6H), 7.26 – 7.15 (m, 4H), 4.86 (s, 1H), 2.28 (s, 6H); ¹³C NMR (101 MHz, DMSO) δ 157.61, 146.64, 142.88, 138.37, 131.32, 130.05, 129.27, 125.61, 120.76, 119.32, 104.34, 33.42, 12.31; HRMS [ESI⁺]: calcd for 514.1004, C₂₇H₂₃BrN₄O₂, [M + H]⁺, found, 515.1082. Purity ≥ 95.0%.

4.4.11. 5-Methyl-4-(naphthalen-1-ylmethylene)-2-phenyl-2,4-dihydro-3H-pyrazol-3-one (b36)

Solid, yield 23%; ¹H NMR (400 MHz, DMSO) δ 8.65 (d, J = 7.1 Hz, 3/5H), 8.54 (s, 1H), 8.33 (d, J = 11.5 Hz, 1H), 8.18 – 7.81 (m, 13/5H), 7.70–7.63 (m, 24/5H), 7.50–7.40 (m, 2H), 7.25–7.17 (m, 1H), 2.48 (s, 3H); ¹³C NMR (101 MHz, DMSO) δ 163.19, 161.77, 152.16, 148.96, 145.21, 144.32, 138.64, 138.39, 133.47, 133.33, 131.96, 131.89, 131.34, 131.27, 130.36, 130.07, 129.77, 129.49, 129.37, 129.29, 129.23, 128.52, 128.35, 128.03, 127.32, 126.93, 125.65, 125.45, 125.16, 125.06, 124.96, 124.54, 118.64, 118.39, 40.64, 40.43, 40.22, 40.01, 39.81, 39.60, 39.39, 17.05, 13.62; HRMS [ESI⁺]: calcd for 312.1263, C₂₁H₁₆N₂O, [M + H]⁺, found, 313.1332. Purity ≥ 95.0%.

4.4.12. 4,4'-(Naphthalen-1-ylmethylene)bis(3-methyl-1-phenyl-1H-pyrazol-5-ol) (bis-b36)

Solid, yield 47%; ¹H NMR (400 MHz, DMSO) δ 8.05–8.04 (m, 1H), 7.94–7.92 (m, 1H), 7.81–7.69 (m, 6H), 7.54 – 7.40 (m, 7H), 7.23–0.21 (d, J = 6.7 Hz, 2H), 5.60 (s, 1H), 2.22 (s, 6H); ¹³C NMR (101 MHz, DMSO) δ 146.13, 137.89, 137.36, 134.17, 131.25, 129.36, 129.27, 127.51, 126.42, 126.27, 125.68, 124.01, 120.83, 12.50, 0.58. HRMS [ESI +]: calcd for 486.2056, C₃₁H₂₆N₄O₂, [M + H]⁺, found, 487.2127. Purity ≥ 95.0%.

4.4.13. 5-Methyl-2-phenyl-4-(2,4,6-tribromo-3-hydroxybenzylidene)-2,4-dihydro-3H-pyrazol-3-one (b52)

Solid, yield 73%; ¹H NMR (400 MHz, DMSO) δ 7.96 (d, J = 11.1 Hz, 1H), 7.93 – 7.69 (m, 3H), 7.44 (dt, J = 25.3, 8.0 Hz, 2H), 7.21 (dt, J = 20.4, 7.4 Hz, 1H), 2.38 (s, 1H), 1.84 (s, 2H); ¹³C NMR (101 MHz, DMSO) δ 160.46, 151.45, 150.57, 144.24, 138.04, 135.37, 134.83, 131.22, 129.42, 125.28, 118.28, 113.19, 112.95, 111.27, 13.37; HRMS [ESI⁺]: calcd for 511.8371, C₁₇H₁₁Br₃N₂O₂, [M + H]⁺, found, 512.3079. Purity ≥ 95.0%.

4.4.14. 5-Methyl-2-phenyl-4-(quinolin-3-ylmethylene)-2,4-dihydro-3H-pyrazol-3-one (b56)

Solid, yield 17%, ¹H NMR (400 MHz, DMSO) δ 9.75 (s, 1H), 9.67 (d, J = 2.0 Hz, 1H), 8.13–8.08 (m, 3H), 7.75–7.71 (m, 3H), 7.73 (t, J = 7.6 Hz, 1H), 7.51 – 7.42 (m, 2H), 7.24 (d, J = 7.4 Hz, 1H), 2.41 (s, 3H); ¹³C NMR (101 MHz, DMSO) δ 192.76, 161.97, 153.92, 152.08, 150.24, 149.26, 148.84, 146.43, 144.88, 141.49, 140.90, 138.48, 133.18, 132.85, 130.41, 130.20, 129.49, 129.36, 129.33, 129.14, 129.05, 128.90, 128.76, 128.40, 128.31, 128.10, 127.93, 127.25, 127.14, 126.95, 126.73, 125.26, 120.57, 118.93, 13.53, 12.67; HRMS [ESI +]: calcd for 313.1215, C₂₀H₁₅N₃O, [M + H]⁺, found, 312.1292. Purity ≥ 95.0%.

4.4.15. 4,4'-(quinolin-3-ylmethylene)bis(3-methyl-1-phenyl-1H-pyrazol-5-ol) (bis-b56)

Solid, yield 36%, ¹H NMR (400 MHz, DMSO) δ 8.82 (d, J = 2.1 Hz, 1H), 8.13 (s, 1H), 7.94 (dd, J = 16.1, 8.2 Hz, 2H), 7.79 (d, J = 8.2 Hz, 4H), 7.67 (t, J = 7.6 Hz, 1H), 7.54 (t, J = 7.5 Hz, 1H), 7.39 (t, J = 8.0 Hz, 4H), 7.18 (t, J = 7.4 Hz, 2H), 5.13 (s, 1H), 2.33 (s, 6H); ¹³C NMR (101 MHz, DMSO) δ 157.81, 152.14, 146.50, 146.40, 139.26, 137.21, 132.79, 129.10, 129.02, 128.90, 128.40, 127.95, 126.94, 124.98, 120.47, 103.20, 32.36, 12.76; HRMS [ESI +]: calcd for 487.2008, C₃₀H₂₅N₅O₂, [M + H]⁺, found, 488.2079. Purity ≥ 95.0%.

4.4.16. 2-(4-Chlorophenyl)-4-(3-hydroxy-4-methoxybenzylidene)-5-methyl-2,4-dihydro-3H-pyrazol-3-one (c37)

Solid, 37%, ¹H NMR (400 MHz, DMSO) δ 9.44 (s, 1H), 8.43 (s, 1H), 8.03 (d, J = 8.5 Hz, 1H), 7.97 (d, J = 8.9 Hz, 2H), 7.68 (s, 1H), 7.49 (d, J = 8.9 Hz, 2H), 7.13 (d, J = 8.5 Hz, 1H), 3.91 (s, 3H), 2.32 (s, 3H). ¹³C NMR (101 MHz, DMSO) δ 162.34, 153.64, 152.72, 149.67, 146.59, 137.73, 129.88, 129.21, 128.52, 126.87, 123.55, 120.44, 120.06, 112.04, 56.29, 13.63. HRMS [ESI +]: calcd for 342.0771, C₁₈H₁₅ClN₂O₃, [M + Na]⁺, found, 365.0667. Purity ≥ 95.0%.

4.4.17. 1-(4-Chlorophenyl)-3-((1-(4-chlorophenyl)-5-hydroxy-3-methyl-1H-pyrazol-4-yl)(3-hydroxy-4-methoxyphenyl)methyl)-4-methyl-1H-pyrazol-5-ol (bis-c37)

Solid, yield 41%, ¹H NMR (400 MHz, DMSO) δ 8.68 (s, 1H), 7.86 (d, J = 8.9 Hz, 4H), 7.42 (d, J = 8.9 Hz, 4H), 6.82 – 6.70 (m, 2H), 6.60 (d, J = 8.3 Hz, 1H), 4.65 (s, 1H), 3.68 (s, 3H), 2.21 (s, 6H). ¹³C NMR (101 MHz, DMSO) δ 147.39, 146.65, 146.42, 134.92, 129.90, 129.37, 129.24, 122.16, 118.06, 115.25, 112.61, 100.00, 56.17, 55.39, 32.76, 12.11. HRMS [ESI +]: calcd for 550.1175, C₂₈H₂₄Cl₂N₄O₄, [M + Na]⁺, found, 573.1028. Purity ≥ 95.0%.

4.4.18. Methyl 4-(3-methyl-4-(4-methylbenzylidene)-5-oxo-4,5-dihydro-1H-pyrazol-1-yl)benzoate (e31)

Solid, yield 28%, ¹H NMR (400 MHz, DMSO) δ 8.53 (d, J = 8.2 Hz, 2H), 8.12 (d, J = 9.0 Hz, 2H), 8.04 (d, J = 9.0 Hz, 2H), 7.85 (s, 1H), 7.41 (d, J = 8.1 Hz, 2H), 3.86 (s, 3H), 2.43 (s, 3H), 2.37 (s, 3H); ¹³C NMR (101 MHz, DMSO) δ 166.21, 162.50, 153.38, 149.50, 145.02, 142.42, 134.61, 130.87, 130.76, 129.88, 125.67, 125.33, 117.69, 52.44, 22.02, 13.64. HRMS [ESI +]: calcd for 334.1317, C₂₀H₁₈N₂O₃, [M + Na]⁺, found, 357.1212. Purity ≥ 95.0%.

4.4.19. Dimethyl 4,4'-((p-tolylmethylene)bis(5-hydroxy-3-methyl-1H-pyrazole-4,1-diy))dibenzoate (bis-e31)

Solid, yield 42%, ¹H NMR (400 MHz, DMSO) δ 8.00 (dd, J = 21.8, 8.9 Hz, 8H), 7.16 (d, J = 8.0 Hz, 2H), 7.03 (d, J = 8.0 Hz, 2H), 4.76 (s, 1H), 3.85 (d, J = 7.5 Hz, 6H), 2.23 (d, J = 8.4 Hz, 9H); ¹³C NMR (101 MHz, DMSO) δ 166.33, 158.41, 148.40, 143.20, 134.90, 130.60, 129.02, 127.56, 125.07, 118.99, 104.45, 52.41, 33.80, 21.00, 12.84. HRMS [ESI +]: calcd for 566.2165, C₃₂H₃₀N₄O₆, [M + Na]⁺, found, 589.2053. Purity ≥ 95.0%.

4.4.20. Methyl 4-(4-(3-methoxybenzylidene)-3-methyl-5-oxo-4,5-dihydro-1H-pyrazol-1-yl)benzoate (**e38**)

Solid, yield 35%, ^1H NMR (400 MHz, DMSO) δ 8.42 (s, 1H), 8.16 – 8.00 (m, 5H), 7.85 (s, 1H), 7.49 (t, $J = 8.0$ Hz, 1H), 7.23 (dd, $J = 8.2$, 2.5 Hz, 1H), 3.85 (d, $J = 2.4$ Hz, 6H), 2.36 (s, 3H); ^{13}C NMR (101 MHz, DMSO) δ 166.20, 162.39, 159.57, 153.40, 149.52, 142.33, 134.54, 130.80, 130.18, 127.37, 126.87, 125.46, 120.34, 118.23, 117.81, 55.82, 52.49, 13.66. HRMS [ESI +]: calcd for 350.1267, $\text{C}_{20}\text{H}_{18}\text{N}_2\text{O}_4$, [M + H] $^+$, found, 351.1351. Purity $\geq 95.0\%$.

4.4.21. Dimethyl 4,4'-(((3-methoxyphenyl)methylene)bis(5-hydroxy-3-methyl-1H-pyrazole-4,1-diyl))dibenzoate (**bis-e38**)

Solid, yield 51%, ^1H NMR (400 MHz, DMSO) δ 7.99 (s, 8H), 7.18 (t, $J = 7.9$ Hz, 1H), 6.89 – 6.81 (m, 2H), 6.74 (d, $J = 7.9$ Hz, 1H), 4.83 (s, 1H), 3.84 (s, 6H), 3.68 (s, 3H), 2.28 (s, 6H); ^{13}C NMR (101 MHz, DMSO) δ 166.25, 159.61, 148.46, 142.56, 130.67, 129.59, 125.59, 120.08, 119.34, 114.27, 110.70, 104.66, 55.31, 52.47, 33.92, 12.61. HRMS [ESI +]: calcd for 582.2114, $\text{C}_{32}\text{H}_{30}\text{N}_4\text{O}_7$, [M + Na] $^+$, found, 605.2004. Purity $\geq 95.0\%$.

4.4.22. Methyl 4-(4-(4-fluorobenzylidene)-3-methyl-5-oxo-4,5-dihydro-1H-pyrazol-1-yl)benzoate (**e42**)

Solid, yield 29%, ^1H NMR (400 MHz, DMSO) δ 8.71 (dd, $J = 8.8$, 5.8 Hz, 2H), 8.07 (dd, $J = 26.6$, 8.8 Hz, 4H), 7.91 (s, 1H), 7.44 (t, $J = 8.8$ Hz, 2H), 3.85 (s, 3H), 2.37 (s, 3H); ^{13}C NMR (101 MHz, CDCl_3) δ 166.84, 166.72, 164.28, 162.15, 151.60, 145.99, 142.07, 136.64, 136.55, 130.55, 129.28, 129.25, 126.73, 126.71, 125.88, 117.72, 117.41, 116.24, 116.02, 52.04, 52.02, 13.34; HRMS [ESI +]: calcd for 338.1067, $\text{C}_{19}\text{H}_{15}\text{FN}_2\text{O}_3$, [M + H] $^+$, found, 339.1145. Purity $\geq 95.0\%$.

4.4.23. Dimethyl 4,4'-(((4-fluorophenyl)methylene)bis(5-hydroxy-3-methyl-1H-pyrazole-4,1-diyl))dibenzoate (**bis-e42**)

Solid, yield 43%, ^1H NMR (400 MHz, DMSO) δ 8.02 (d, $J = 8.9$ Hz, 4H), 7.96 (d, $J = 8.9$ Hz, 4H), 7.28 (dd, $J = 8.4$, 5.7 Hz, 2H), 7.09 (t, $J = 8.8$ Hz, 2H), 4.93 (s, 1H), 3.85 (s, 6H), 2.31 (s, 6H); ^{13}C NMR (101 MHz, CDCl_3) δ 166.72, 162.76, 160.32, 147.98, 141.10, 136.03, 130.51, 128.73, 128.65, 126.71, 119.67, 117.85, 115.29, 115.08, 106.25, 52.23, 33.07, 11.96; HRMS [ESI +]: calcd for 570.1915, $\text{C}_{31}\text{H}_{27}\text{FN}_4\text{O}_6$, [M + Na] $^+$, found, 593.1811. Purity $\geq 95.0\%$.

4.4.24. Methyl 4-(3-methyl-5-oxo-4-(3-(trifluoromethoxy)benzylidene)-4,5-dihydro-1H-pyrazol-1-yl)benzoate (**e43**)

Solid, yield 32%, ^1H NMR (400 MHz, DMSO) δ 8.66 (d, $J = 7.9$ Hz, 7/10H), 8.14 – 7.80 (m, 63/10H), 7.76–7.71 (m, 1H), 7.59–7.54 (m, 2H), 3.85 (s, 3H), 2.36 (s, 21/10H), 2.05 (s, 9/10H); ^{13}C NMR (101 MHz, DMSO) δ 166.15, 161.68, 152.62, 142.07, 140.06, 134.92, 133.38, 130.79, 130.53, 129.03, 127.54, 125.57, 121.37, 118.97, 117.67, 117.51, 52.47, 13.31; HRMS [ESI $^+$]: calcd for 404.0984, $\text{C}_{20}\text{H}_{15}\text{F}_3\text{N}_2\text{O}_4$, [M + H] $^+$, found, 405.1055. Purity $\geq 95.0\%$.

4.4.25. Dimethyl 4,4'-(((3-(trifluoromethoxy)phenyl)methylene)bis(5-hydroxy-3-methyl-1H-pyrazole-4,1-diyl))dibenzoate (**bis-e43**)

Solid, yield 49%; ^1H NMR (400 MHz, DMSO) δ 7.98 (dd, $J = 27.8$, 8.9 Hz, 8H), 7.75 (s, 1H), 7.43 – 7.23 (m, 3H), 5.09 (s, 1H), 3.85 (s, 6H), 2.25 (s, 6H); ^{13}C NMR (101 MHz, DMSO) δ 166.22, 158.59, 147.71, 146.32, 142.35, 134.89, 130.67, 128.52, 127.22, 125.74, 122.05, 120.10, 119.50, 103.64, 100.00, 52.47, 28.95, 12.22; HRMS [ESI $^+$]: calcd for 636.1832, $\text{C}_{32}\text{H}_{27}\text{F}_3\text{N}_4\text{O}_7$, [M + Na] $^+$, found, 659.1731. Purity $\geq 95.0\%$.

4.4.26. Methyl 4-(4-(3-hydroxybenzylidene)-3-methyl-5-oxo-4,5-dihydro-1H-pyrazol-1-yl)benzoate (**e59**)

Solid, yield 28%; ^1H NMR (400 MHz, DMSO) δ 9.87 (d, $J = 39.4$ Hz, 1H), 8.22 – 8.00 (m, 23/5H), 7.92 (t, $J = 8.4$ Hz, 7/5H), 7.78 (s, 7/10H), 7.38 (t, $J = 7.9$ Hz, 13/10H), 7.06 (dd, $J = 8.1$, 2.3 Hz, 7/10H), 6.97 (t, $J = 7.8$ Hz, 3/10H), 3.84 (d, $J = 10.5$ Hz, 3H), 2.36 (s, 23/10H), 2.18 (s, 7/

10H). ^{13}C NMR (101 MHz, DMSO) δ 166.20, 162.33, 157.79, 153.40, 149.89, 142.38, 134.45, 130.78, 130.06, 126.45, 125.98, 125.37, 121.38, 120.13, 117.70, 52.47, 13.64. HRMS [ESI $^+$]: calcd for 336.1110, $\text{C}_{19}\text{H}_{16}\text{N}_2\text{O}_4$, [M + Na] $^+$, found, 359.1004. Purity $\geq 95.0\%$.

4.4.27. Dimethyl 4,4'-(((3-hydroxyphenyl)methylene)bis(5-hydroxy-3-methyl-1H-pyrazole-4,1-diyl))dibenzoate (**bis-e59**)

Solid, yield 47%; ^1H NMR (400 MHz, DMSO) δ 9.09 (s, 1H), 8.07 (d, $J = 8.8$ Hz, 4H), 7.96 (d, $J = 8.9$ Hz, 4H), 6.99 (t, $J = 7.8$ Hz, 1H), 6.73 (s, 1H), 6.68 (d, $J = 7.8$ Hz, 1H), 6.50 (d, $J = 8.0$ Hz, 1H), 4.67 (s, 1H), 3.84 (s, 6H), 2.22 (s, 6H); ^{13}C NMR (101 MHz, DMSO) δ 166.37, 158.39, 157.53, 148.46, 146.13, 143.60, 130.56, 129.23, 124.80, 118.86, 118.43, 114.72, 112.95, 103.97, 52.40, 34.18, 13.00. HRMS [ESI $^+$]: calcd for 568.1958, $\text{C}_{31}\text{H}_{28}\text{N}_4\text{O}_7$, [M + Na] $^+$, found, 591.1854. Purity $\geq 95.0\%$.

4.5. PHGDH enzymatic activity assay

PHGDH activity was tested in 96-well plates at room temperature by measuring NADH production mediated by PHGDH through the diaphorase-mediated reduction of resazurin. Hydrazine sulfate was included to prevent product inhibition of PHGDH. PHGDH assay buffer contained 30 mM Tris 8.0 and 1 mM EDTA. Substrates and enzyme concentrations were as follows: 200 nM PHGDH 1–314, mixtures (0.1 mM resazurin; 0.001 U/ μL diaphorase; 1 mM hydrazine sulfate; 20 μM NAD $^+$; 0.1 mM 3-PG). Compounds and PHGDH were preincubated for 2 h, and then the mixtures were added. The 96-well plate was shaken evenly and incubated in dark for 1 h. The resulting fluorescence was measured using a Synergy H1 Hybrid Multi-Mode Reader (BioTek) at Ex/Em = 550/590 nm. PHGDH inhibition data were calculated by the following formula: inhibition rate = $1 - (\text{F}_{\text{compound}} - \text{F}_{\text{No-3PG}}) / (\text{F}_{\text{DMSO}} - \text{F}_{\text{No-3PG}})$. F_{DMSO} was resorufin fluorescence of compound well; F_{DMSO} was resorufin fluorescence of DMSO well, and $\text{F}_{\text{No-3PG}}$ was resorufin fluorescence of non-substrate well. IC $_{50}$ values were calculated by Graph-Pad Prism 7.0 software using XY modeling.

For inhibition mode measurements, compounds and enzyme were pre-incubated for 2 h. Then, we added different concentrations of the substrate mixed solution, and read the fluorescence value every two minutes at room temperature for a total of 20 min, finally, used Prism to fit the initial rate plots.

4.6. Cell culture

The cell lines, including human breast cancer cell line MDA-MB-468 and Hs578T, human ovarian cancer cell line A2780 and SKOV3, and normal cell line MCF-10A were obtained from American Type Culture Collection (ATCC; Manassas, VA, USA). The cells were cultured in Dubelco's Modified Eagle Medium (DMEM) supplemented with 10% fetal bovine serum (FBS) and grown in a CO $_2$ incubator at 37 $^{\circ}\text{C}$ with a humidified atmosphere of 5% CO $_2$ and 95% air according to ATCC guidelines.

4.7. Cell viability assay

MDA-MB-468, Hs578T, A2780, and SKOV3 cells were seeded (2–10 $\times 10^3$ cells per well) into 96-well plates. After incubation for 24 h, the cells were treated with serially diluted compounds for 96 h. Cell viability was determined by using MTT assay. Briefly, 20 μL of MTT reagent (5 mg/mL) was added to each of the wells and then incubated for 2–4 h. The absorbance was measured at 570 nm using a Microplate Reader 3550-UV (ThermoFisher Scientific).

In the format supplementation experiment, the appropriate media was added to cells, which included vehicle (DMSO), or b36 and formate (1 mM). Each experiment was repeated three times. The IC $_{50}$ value of compounds was defined as the concentration of the compounds required to inhibit cell proliferation by 50% relative to the untreated controls, as

determined by non-linear curve fitting of the experimental data and calculated using GraphPad Prism 7.0 software.

4.8. *In silico* ADMET prediction

To explore the pharmacokinetics of the best active compounds, we used the Qikprop program (Schrödinger, 2018–1) to predict their ADMET properties. All the compounds were prepared from LigPrep and calculated by their pharmacokinetic properties with Qikprop. Finally, we obtained physically significant descriptors and pharmaceutically relevant properties, including octanol/water partitioning coefficient, aqueous solubility, intestinal wall permeability, plasma protein binding, and others.

4.9. Serine and glycine level detection

4.9.1. Sample preparation and derivatization

MDA-MB-468 cells were seeded (2×10^5 cells per well) in 6-well plates and allowed to attach for 24 h, then treated with compound **b36** or vehicle (DMSO) for 48 h. The media was removed by aspiration, and the cells were washed twice with PBS. Metabolome extraction was performed by adding 500 μ L of ice-cold extraction solvent (methanol: water = 1:1) and was repeatedly freeze-thawed 3 times by liquid nitrogen, then centrifuged (20 min, 20000 rpm, 4 °C). Finally, the supernatant was collected and dried with a nitrogen blowing instrument and dissolved in methanol: water (1:1) for derivatization. The sample' derivatization was carried out strictly according to the instruction of the AccQTag Ultra reagent pack (waters). The resulting supernatant was frozen on dry ice and kept at -80 °C until LC-MS/MS analysis.

4.9.2. UPLC-MS/MS analyses

The chromatographic separation was achieved by injecting 2 μ L of sample on a reversed-phase gradient chromatography column (ACQUITY UPLC BEH amide, 2.1 mm \times 100 mm, 1.7 μ m, Waters). Mobile phase A consisted of 0.1% formic acid in water (v/v), and mobile Phase B was 0.1% formic acid in acetonitrile (v/v). The column compartment was maintained at 25 °C, and the autosampler sample tray was set to 4 °C. The linear gradient elution was performed at 0.4 mL/min, and the mobile phase gradient (%B) was as follows: 0 min 3%, 1 min 3%, 2 min 13%, 5.5 min 15%, 6.5 min 60% for 1 min, and finally returning to 3% B (1.3 min) for re-equilibration. The weak and the intense washes were 90:10 water/acetonitrile (v/v) and 100% 10:90 water/acetonitrile. The mass spectrometer was via electrospray ionization (ESI) in positive ion mode and used nitrogen as the dissolvent gas and argon as the collision gas. All mobile phase was introduced into the generic source, and the conditions were: capillary voltage, 1.5 kV; source offset, 50 V; desolvation temperature, 500 °C; source temperature, 150 °C, desolvation gas flow, 1000 L/h; cone gas flow, 150 L/h; nebulizer gas, 7.0 bar; collision gas, 0.15 mL/min. The raw data were processed by the TargetLynx application package within MassLynx software (Waters), and the mean smoothed, and peak integration was performed using the ApexTrak algorithm. Further statistical analysis was performed on the resulting calculated concentrations using Graph-Pad Prism 7.0.

4.10. EdU incorporation assay

The MDA-MB-468 cells were seeded (6000 per well) into 96-well plates and left to adhere overnight. The cells were treated with different concentrations of **b36** in DMSO as a vehicle (<0.1%) for 48 h. The cells were then incubated with 50 μ M EdU for 2 h, followed by washed twice with PBS and fixed using 4% paraformaldehyde (PFA) for 30 min. Next, the cells were incubated with glycine for 5 min to remove the residual paraformaldehyde, washed with PBS to neutralize PFA, and incubated with 0.5% Triton X-100 in PBS. The cells were incubated for 30 min with 1 \times Apollo® dye staining reaction in the dark and washed with PBS 2–5 times. At last, the cells were incubated with 5 μ g/mL

Hoechst 33342 at room temperature for 10 min, followed by observation under a fluorescence microscope (Thermo Fisher Scientific).

4.11. Cell cycle assay

MDA-MB-468 cells were seeded (2×10^5 cells per well) in a 6-well plate and treated with compound **b36** or vehicle (DMSO) for 48 h. After incubation, the cells were harvested and washed with ice-cold PBS. Cell cycle progression was analyzed using propidium iodide (PI) (50 mg/L, RNase free) staining. Then stained cells were analyzed using an Attune NxT Flow Cytometer (Thermo Fisher Scientific), and data were analyzed using the FlowJo software.

4.12. Western blot

MDA-MB-468 cells (2.0×10^5) were seeded in a 6-well plate and treated with compound **b36** or vehicle (DMSO) for 48 h. Subsequently, the treated cells were lysed and boiled for 10 min. Proteins were separated by SDS-PAGE, transferred to a PVDF membrane, and detected with relevant antibodies against γ H2AX or GAPDH.

4.13. Immunofluorescence and quantification

MDA-MB-468 cells (3×10^5 cells in a six-well plate containing coverslips) were treated with DMSO or compound **b36** for 48 h, and then cells were fixed in pre-cold 4% paraformaldehyde for 20 min, washed three times in 1 \times PBS, and then extracted with 0.1% Triton X-100 PBS solution for 5 min, then blocked in PBS containing 1.5% bovine serum albumin (BSA) for 20 min at room temperature, and then incubated sequentially with primary antibody against phospho-H2AX (1:1000 dilution) at 4 °C overnight. Cells were washed three times with 1 \times PBS and incubated with Alexa Fluor 568-conjugated secondary antibody (Thermo Fisher Scientific) at room temperature for 1 h. The cells were then stained with DAPI (1 μ g/mL) and the confocal images were acquired using an Olympus SpinSR10 laser scanning microscope. Cells that displayed 20 or more discrete bright dots were considered positive for γ -H2AX foci which were quantified using Fiji. Foci pictures of each individual experiment were obtained with the same exposure parameters.

Author contributions

YLZ, YFL, and QXS designed the experiment scheme. XZ did the synthesis. The high-throughput screening was done by XZ, TPT, LT, and YZ; XZ, KG, YPT and YL performed the assays. XZ and KG were responsible for drafting the manuscript and drawing the figures of this article. YLZ and YFL edited and revised the manuscript. All authors reviewed and approved the final version of the manuscript.

Declaration of Competing Interest

The authors declare that they have no known competing financial interests or personal relationships that could have appeared to influence the work reported in this paper.

Acknowledgements

This work was supported by the Project of National S&T Major Project (2018ZX09201018), National Natural Sciences Foundation of China (81773198) and the National Key R&D Program of China (2016YFC1303200).

Appendix A. Supplementary material

Supplementary data to this article can be found online at <https://doi.org/10.1016/j.bioorg.2021.105159>.

References

- [1] D. Hanahan, R.A. Weinberg, Hallmarks of cancer: the next generation, *Cell* 144 (5) (2011) 646–674.
- [2] A. Schulze, A.L. Harris, How cancer metabolism is tuned for proliferation and vulnerable to disruption, *Nature* 491 (7424) (2012) 364–373.
- [3] O. Warburg, On the origin of cancer cells, *Science* 123 (3191) (1956) 309–314.
- [4] K.R. Mattaini, M.R. Sullivan, M.G. Vander Heiden, The importance of serine metabolism in cancer, *J. Cell Biol.* 214 (3) (2016) 248–257.
- [5] M. Palacin, R. Estevez, J. Bertran, A. Zorzano, Molecular biology of mammalian plasma membrane amino acid transporters, *Physiol. Rev.* 78 (4) (1998) 969–1054.
- [6] R.J. DeBerardinis, J.J. Lum, G. Hatzivassiliou, C.B. Thompson, The biology of cancer: Metabolic reprogramming fuels cell growth and proliferation, *Cell Metab.* 7 (1) (2008) 11–20.
- [7] G.S. Ducker, J.D. Rabinowitz, One-Carbon Metabolism in Health and Disease, *Cell Metab.* 25 (1) (2017) 27–42.
- [8] D. Samanta, Y. Park, S.A. Andrabi, L.M. Shelton, D.M. Gilkes, G.L. Semenza, PHGDH Expression Is Required for Mitochondrial Redox Homeostasis, Breast Cancer Stem Cell Maintenance, and Lung Metastasis, *Cancer Res.* 76 (15) (2016) 4430–4442.
- [9] R. Possemato, K.M. Marks, Y.D. Shaul, M.E. Pacold, D. Kim, K. Birsoy, S. Sethumadhavan, H.K. Woo, H.G. Jang, A.K. Jha, W.W. Chen, F.G. Barrett, N. Stransky, Z.Y. Tsun, G.S. Cowley, J. Barretina, N.Y. Kalaany, P.P. Hsu, K. Ottina, A.M. Chan, B. Yuan, L.A. Garraway, D.E. Root, M. Mino-Kenudson, E.F. Brachtel, E. M. Driggers, D.M. Sabatini, Functional genomics reveal that the serine synthesis pathway is essential in breast cancer, *Nature* 476 (7360) (2011) 346–350.
- [10] R. Beroukhi, C.H. Mermel, D. Porter, G. Wei, S. Raychaudhuri, J. Donovan, J. Barretina, J.S. Boehm, J. Dobson, M. Urashima, K.T. Mc Henry, R.M. Pinchback, A.H. Ligon, Y.J. Cho, L. Haery, H. Greulich, M. Reich, W. Winckler, M.S. Lawrence, B.A. Weir, K.E. Tanaka, D.Y. Chiang, A.J. Bass, A. Loo, C. Hoffman, J. Prensner, T. Liefeld, Q. Gao, D. Yecies, S. Signoretti, E. Maher, F.J. Kaye, H. Sasaki, J. E. Tepper, J.A. Fletcher, J. Tabernero, J. Baselga, M.S. Tsao, F. Demicheli, M. A. Rubin, P.A. Janne, M.J. Daly, C. Nucera, R.L. Levine, B.L. Ebert, S. Gabriel, A. K. Rustgi, C.R. Antonescu, M. Ladanyi, A. Letai, L.A. Garraway, M. Loda, D.G. Beer, L.D. True, A. Okamoto, S.L. Pomeroy, S. Singer, T.R. Golub, E.S. Lander, G. Getz, W.R. Sellers, M. Meyerson, The landscape of somatic copy-number alteration across human cancers, *Nature* 463 (7283) (2010) 899–905.
- [11] J.W. Locasale, A.R. Grassian, T. Melman, C.A. Lyssiotis, K.R. Mattaini, A.J. Bass, G. Haffner, C.M. Metallo, T. Muranen, H. Sharf, A.T. Sasaki, D. Anastasiou, E. Mullarky, N.I. Vokes, M. Sasaki, R. Beroukhi, G. Stephanopoulos, A.H. Ligon, M. Meyerson, A.L. Richardson, L. Chin, G. Wagner, J.M. Asara, J.S. Brugge, L. C. Cantley, M.G. Vander Heiden, Phosphoglycerate dehydrogenase diverts glycolytic flux and contributes to oncogenesis, *Nat. Genet.* 43 (9) (2011) 869–874.
- [12] X.Y. Zhao, J.F. Fu, J.L. Du, W.X. Xu, The Role of D-3-Phosphoglycerate Dehydrogenase in Cancer, *Int. J. Biol. Sci.* 16 (9) (2020) 1495–1506.
- [13] J. Zhang, H. Wei, X. Liu, N. Wang, Y.F. Qi, Y. Zhang, S.L. Zhang, Downregulation of phosphoglycerate dehydrogenase inhibits proliferation and enhances cisplatin sensitivity in cervical adenocarcinoma cells by regulating Bcl-2 and caspase-3, *Cancer Biol. Ther.* 16 (4) (2015) 541–548.
- [14] X.Q. Jia, S. Zhang, H.J. Zhu, W. Wang, J.H. Zhu, X.D. Wang, J.F. Qiang, Increased Expression of PHGDH and Prognostic Significance in Colorectal Cancer, *Transl. Oncol.* 9 (3) (2016) 191–196.
- [15] G.M. DeNicola, P.H. Chen, E. Mullarky, J.A. Sudderth, Z.P. Hu, D. Wu, H. Tang, Y. Xie, J.M. Asara, K.E. Huffman, I.I. Wistuba, J.D. Minna, R.J. DeBerardinis, L. C. Cantley, NRF2 regulates serine biosynthesis in non-small cell lung cancer, *Nat. Genet.* 47 (12) (2015) 1475–1481.
- [16] Z.W. Song, C. Feng, Y.L. Lu, Y. Lin, C.Y. Dong, PHGDH is an independent prognosis marker and contributes cell proliferation, migration and invasion in human pancreatic cancer, *Gene* 642 (2018) 43–50.
- [17] J.L. Liu, S.L. Guo, Q.Z. Li, L.X. Yang, Z.B. Xia, L.J. Zhang, Z.S. Huang, N. Zhang, Phosphoglycerate dehydrogenase induces glioma cells proliferation and invasion by stabilizing forkhead box M1, *J. Neuro-Oncol.* 111 (3) (2013) 245–255.
- [18] J. Fan, X. Teng, L. Liu, K.R. Mattaini, R.E. Looper, M.G. Vander Heiden, J. D. Rabinowitz, Human phosphoglycerate dehydrogenase produces the oncometabolite D-2-hydroxyglutarate, *ACS Chem. Biol.* 10 (2) (2015) 510–516.
- [19] E. Mullarky, N.C. Lucki, R. Beheshti Zavareh, J.L. Anglin, A.P. Gomes, B. N. Nicolay, J.C. Wong, S. Christen, H. Takahashi, P.K. Singh, J. Blenis, J.D. Warren, S.M. Fendt, J.M. Asara, G.M. DeNicola, C.A. Lyssiotis, L.L. Lairson, L.C. Cantley, Identification of a small molecule inhibitor of 3-phosphoglycerate dehydrogenase to target serine biosynthesis in cancers, *Proc. Natl. Acad. Sci. U S A* 113 (7) (2016) 1778–1783.
- [20] M.E. Pacold, K.R. Brimacombe, S.H. Chan, J.M. Rohde, C.A. Lewis, L.J.Y.M. Swier, R. Possemato, W.W. Chen, L.B. Sullivan, B.P. Fiske, S. Cho, E. Freinkman, K. Birsoy, M. Abu-Remaileh, Y.D. Shaul, C.M. Liu, M. Zhou, M.J. Koh, H. Chung, S.M. Davidson, A. Luengo, A.Q. Wang, X. Xu, A. Yasgar, L. Liu, G. Rai, K.D. Westover, M. G. Vander Heiden, M. Shen, N.S. Gray, M.B. Boxer, D.M. Sabatini, A PHGDH inhibitor reveals coordination of serine synthesis and one-carbon unit fate (vol 12, pg 452, 2016), *Nat. Chem. Biol.* 12(8) (2016) 656–656.
- [21] S. Ravez, C. Corbet, Q. Spillier, A. Dutu, A.D. Robin, E. Mullarky, L.C. Cantley, O. Feron, R. Frederick, alpha-Ketothioamide Derivatives: A Promising Tool to Interrogate Phosphoglycerate Dehydrogenase (PHGDH), *J. Med. Chem.* 60 (4) (2017) 1591–1597.
- [22] Q. Wang, M.V. Libert, P. Liu, X.B. Deng, Y. Liu, J.W. Locasale, L.H. Lai, Rational Design of Selective Allosteric Inhibitors of PHGDH and Serine Synthesis with Antitumor Activity, *Cell Chem. Biol.* 24 (1) (2017) 55–65.
- [23] J.E. Unterlass, A. Baslé, T.J. Blackburn, J. Tucker, C. Cano, M.E.M. Noble, N. J. Curtin, Validating and enabling phosphoglycerate dehydrogenase (PHGDH) as a target for fragment-based drug discovery in PHGDH-amplified breast cancer, *Oncotarget* 9 (17) (2018) 13139–13153.
- [24] I.M. Raze Therapeutics, N. Moyer, M. P 3-Phosphoglycerate Dehydrogenase Inhibitors and Uses Thereof, 2017.
- [25] H. Weinstabl, M. Treu, J. Rinnenthal, S.K. Zahn, P. Ettmayer, G. Bader, G. Dahmann, D. Kessler, K. Rumpel, N. Mischerikow, F. Savarese, T. Gerstberger, M. Mayer, A. Zoepfel, R. Schnitzer, W. Sommergruber, P. Martinelli, H. Arnhof, B. Peric-Simov, K.S. Hofbauer, G. Gavel, Y. Scherbantini, S. Mitzner, T.N. Fetz, G. Scholz, J. Bruchhaus, M. Burkard, R. Kousek, T. Ciftci, B. Sharps, A. Schrenk, C. Harrer, D. Haering, B. Wolkerstorfer, X. Zhang, X. Lv, A. Du, D. Li, Y. Li, J. Quant, M. Pearson, D.B. McConnell, Intracellular Trapping of the Selective Phosphoglycerate Dehydrogenase (PHGDH) Inhibitor BI-4924 Disrupts Serine Biosynthesis, *J. Med. Chem.* 62 (17) (2019) 7976–7997.
- [26] S.M. Paul, D.S. Mytelka, C.T. Dunwiddie, C.C. Persinger, B.H. Munos, S. R. Lindborg, A.L. Schacht, How to improve R&D productivity: the pharmaceutical industry's grand challenge, *Nat. Rev. Drug Discov.* 9 (3) (2010) 203–214.
- [27] G. Karageorgis, S. Warriner, A. Nelson, Efficient discovery of bioactive scaffolds by activity-directed synthesis, *Nat. Chem.* 6 (10) (2014) 872–876.
- [28] R. Liu, X. Li, K.S. Lam, Combinatorial chemistry in drug discovery, *Curr. Opin. Chem. Biol.* 38 (2017) 117–126.
- [29] J. Fan, J. Ye, J.J. Kamphorst, T. Shlomi, C.B. Thompson, J.D. Rabinowitz, Quantitative flux analysis reveals folate-dependent NADPH production, *Nature* 510 (7504) (2014) 298–302.
- [30] N. Gray, R. Zia, A. King, V.C. Patel, J. Wendon, M.J.W. McPhail, M. Coen, R. S. Plumb, I.D. Wilson, J.K. Nicholson, High-Speed Quantitative UPLC-MS Analysis of Multiple Amines in Human Plasma and Serum via Precolumn Derivatization with 6-Aminoquinolyl-N-hydroxysuccinimidyl Carbamate: Application to Acetaminophen-Induced Liver Failure, *Anal. Chem.* 89 (4) (2017) 2478–2487.
- [31] C.X. Song, C. He, Bioorthogonal labeling of 5-hydroxymethylcytosine in genomic DNA and diazirine-based DNA photo-cross-linking probes, *Acc. Chem. Res.* 44 (9) (2011) 709–717.
- [32] J.K. Dong, H.M. Lei, Q. Liang, Y.B. Tang, Y. Zhou, Y. Wang, S.Z. Zhang, W.B. Li, Y. G. Tong, G.L. Zhuang, L. Zhang, H.Z. Chen, L. Zhu, Y. Shen, Overcoming erlotinib resistance in EGFR mutation-positive lung adenocarcinomas through repression of phosphoglycerate dehydrogenase, *Theranostics* 8 (7) (2018) 1808–1823.
- [33] S. Tsuda, N. Matsusaka, S. Ueno, N. Susa, Y.F. Sasaki, The influence of antioxidants on cigarette smoke-induced DNA single-strand breaks in mouse organs: a preliminary study with the alkaline single cell gel electrophoresis assay, *Toxicol. Sci.* 54 (1) (2000) 104–109.
- [34] E.M. Bowers, G. Yan, C. Mukherjee, A. Orry, L. Wang, M.A. Holbert, N.T. Crump, C. A. Hazzalin, G. Liszczak, H. Yuan, C. Laroocca, S.A. Saldanha, R. Abagyan, Y. Sun, D. J. Meyers, R. Marmorstein, L.C. Mahadevan, R.M. Alani, P.A. Cole, Virtual ligand screening of the p300/CBP histone acetyltransferase: identification of a selective small molecule inhibitor, *Chem. Biol.* 17 (5) (2010) 471–482.